nature neuroscience

Article

https://doi.org/10.1038/s41593-022-01226-y

Contextual and pure time coding for self and other in the hippocampus

Received: 10 April 2022

Accepted: 31 October 2022

Published online: 30 December 2022

Check for updates

David B. Omer [1,2] ✉, Liora Las[1] & Nachum Ulanovsky [1] ✉

Navigation and episodic memory depend critically on representing temporal sequences. Hippocampal 'time cells' form temporal sequences, but it is unknown whether they represent context-dependent experience or time per se. Here we report on time cells in bat hippocampal area CA1, which, surprisingly, formed two distinct populations. One population of time cells generated different temporal sequences when the bat hung at different locations, thus conjunctively encoding spatial context and time—'contextual time cells'. A second population exhibited similar preferred times across different spatial contexts, thus purely encoding elapsed time. When examining neural responses after the landing moment of another bat, in a social imitation task, we found time cells that encoded temporal sequences aligned to the other's landing. We propose that these diverse time codes may support the perception of interval timing, episodic memory and temporal coordination between self and others.

The hippocampal formation is essential for navigation and episodic memory[1–5]. Both depend critically on coding of temporal sequences. Extensive research has revealed hippocampal time cells that encode temporal sequences[6–17]—neurons that fire transiently and sequentially at specific times. Such time cells were found both in rodents[6–17] and in humans[18]. Previous studies have reported on 're-timing' of time cells in different contexts—for example, under different behaviors, in different environments or when exposed to different odors[6,7,12,16,17]. However, relatively little is known about the representation of time in different spatial contexts—a question that is of great interest because space and time are two cardinal variables that are encoded in the hippocampus[19–23]. Furthermore, although social-spatial representations have been found in rodents[24], bats[25] and humans[26], nothing is known about how the brain encodes time in a social situation. In this study, we set out to close these gaps, by investigating the neuronal representations of time for self and other, in different spatial contexts.

Results

Time cells in the bat hippocampus

We conducted neuronal recordings from dorsal hippocampal area CA1 of Egyptian fruit bats (*Rousettus aegyptiacus*) that were engaged in an observational learning task[25]. We placed three landing balls at three different locations in the room: A, B and Start (Fig. 1a,b). Bats were trained in pairs—an observer and a demonstrator (four pairs in total). The demonstrator bat was trained to fly roughly randomly from the start ball to ball A or B, land on it and then take off and fly back to the start ball. The observer bat was trained to watch and remember the demonstrator's ball choice and imitate it after a delay of several seconds (Fig. 1b,c and Extended Data Fig. 1a–c). The observer bat was rewarded with fruit on all correct trials but not on incorrect trials (Methods). The stationary delay times on the balls (after landing) were highly variable (Fig. 1d), because the bats took off voluntarily. We used a tetrode-based microdrive and a wireless electrophysiology system to record single-neuron activity in dorsal hippocampal area CA1 of the observer bat. In this study, we analyzed data only when both bats were hanging motionlessly on one of the landing balls (Fig. 1b, and Fig. 1c: the epochs are marked by red rectangles for the observer and blue rectangles for the demonstrator). Note that during the time that the bats were hanging from the landing balls, they voluntarily did not move. We used the landing moment as a reference time ($t = 0$) for aligning the CA1 neuronal activity. This allowed us to define six conditions—2 bats (observer or demonstrator landing) × 3 locations (Extended Data Fig. 1b)—and, thus, measure the activity of time cells in the observer's CA1 aligned to the landing moments of each bat, in three different locations in the room. To our knowledge, this is the first study that investigated time cells at different locations, within the same environment.

[1]Department of Brain Sciences, Weizmann Institute of Science, Rehovot, Israel. [2]Edmond and Lily Safra Center for Brain Sciences, Hebrew University of Jerusalem, Jerusalem, Israel. ✉e-mail: david.omer@mail.huji.ac.il; nachum.ulanovsky@weizmann.ac.il

https://doi.org/10.1038/s41593-022-01226-y

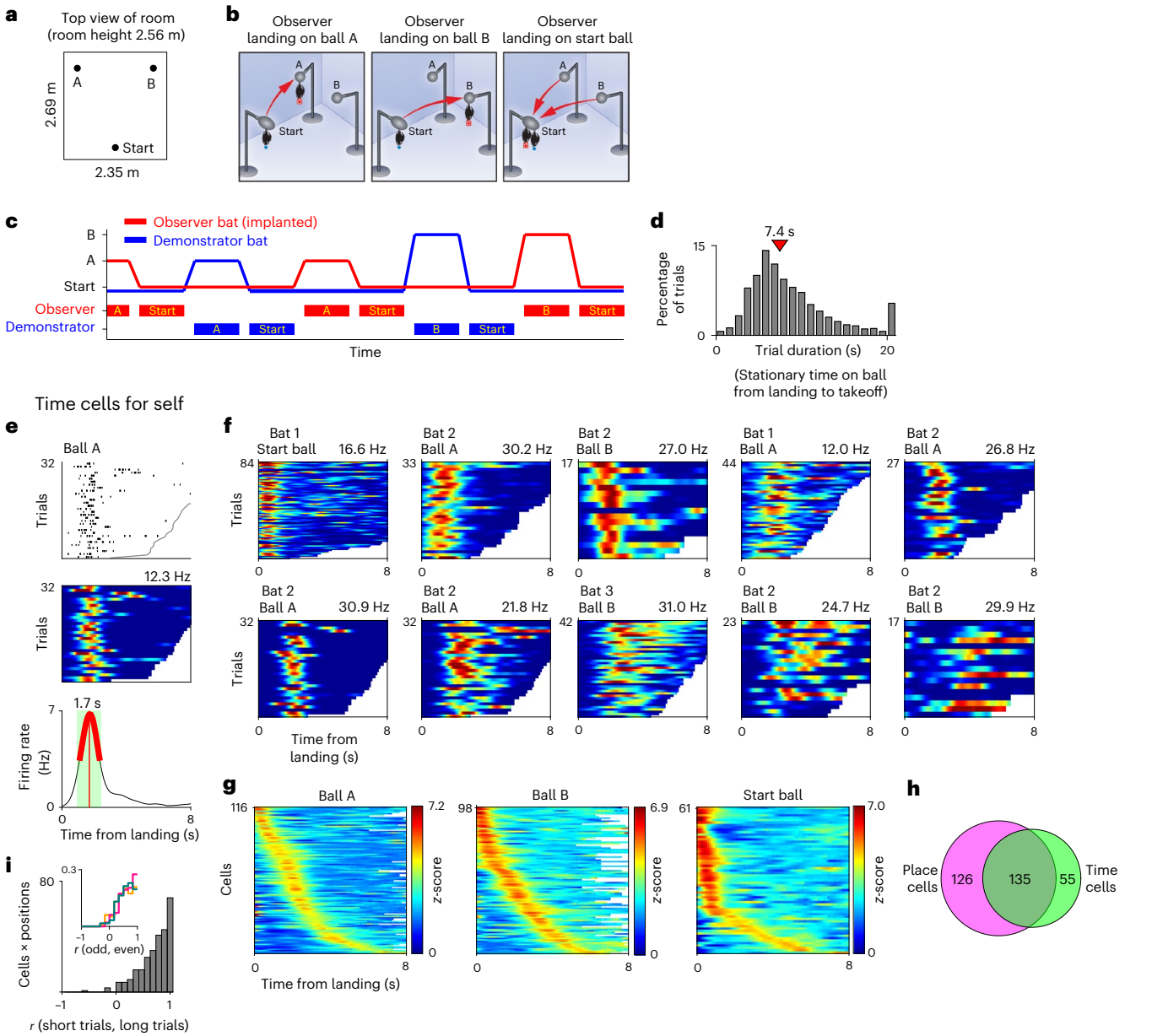

Fig. 1 | Time cells in bat hippocampal area CA1. a, Top view of experimental room. Three landing balls were positioned inside the room, designated 'Start', 'A' and 'B'. **b**, The three conditions that were used to analyze and align self time cells. **c**, Schematic ethogram describing the behavioral task. An observer bat (red) and a demonstrator bat (blue) flew alternatingly from the start ball to either ball A or ball B and back. Here we analyzed only epochs when both bats were hanging motionlessly on the landing balls, with each epoch starting at the landing moment of one of the bats (colored rectangles at bottom). **d**, Distribution of trial durations (time spent by the observer bat on the landing ball, from landing to takeoff, pooled over the three balls); the last bin corresponds to trial durations ≥20 seconds. Median trial duration: 7.4 seconds (red arrowhead). **e**, Example time cell. Top, spike raster: *x* axis, elapsed time from the moment the bat has landed (time 0); *y* axis, repeated landings (trials). Each line in the raster represents the spiking activity in a single trial; each tick represents one spike. Trials were sorted according to trial duration; the thin gray line denotes the trial end (shown are only spikes contained within the trial). Middle, color-coded raster showing the instantaneous firing rate in each trial, arranged as the spike raster above. Color scale ranges from zero (blue) to the maximal firing rate in the panel (red; maximal rate). Bottom: Temporal tuning curve (black trace), which is the averaged firing rate of the neuron (average of the color-coded raster above). Preferred time is indicated above the peak firing (marked also by vertical red line). Green shading: statistically significant time bins. Red curve: width at half height of the time field. **f**, Color-coded rasters for additional ten examples of time cells, showing instantaneous firing rate on single trials: *x* axis, elapsed time from the landing moment (time 0); *y* axis, repeated landings (trials), sorted according to trial duration. Each raster corresponds to a single location in the room (indicated above the raster), and each line in the raster represents the instantaneous firing rate of the cell in each trial, in 100-ms bins; color scale ranges from zero (blue) to the maximal firing rate in each panel (red; the maximal rate is indicated above the raster). Cells are arranged according to preferred time, from top left to bottom right. Both rewarded (correct) and non-rewarded (incorrect) trials were included in the rasters in **e** and **f** and in all the rasters in the paper. See additional 20 examples in Extended Data Fig. 3. **g**, Firing sequences formed by time cells in each of the three locations in the room (balls A, B and Start). *x* axis, elapsed time from the landing moment; *y* axis, temporal tuning curve of each time cell, averaged across trials, sorted by the cell's preferred time, and *z*-scored. Color scale ranges from zero (blue) to the maximal *z*-scored firing rate across all the neurons for each location (red). **h**, Venn diagram: total numbers of time cells and place cells (circle areas in the Venn are scaled according to the indicated values, here and in all Venn diagrams elsewhere). **i**, Time cells exhibited stable tuning. Main panel: high Pearson correlations between the neuron's temporal tuning curve in short trials, with duration < median trial duration, versus long trials ≥ median trial duration ($n = 274$ cells × positions; *y* axis shows counts; median of correlations: $r = 0.73$). Inset: distribution of Pearson correlations between odd and even trials for time cells tuned on ball A (orange line), ball B (blue) and start ball (red), showing stability of time tuning across trials at each location (*y* axis, fraction).

We first examined time cells in the observer bat relative to its own landings (Fig. 1b). Out of a total of 391 well-isolated cells, 190 neurons (48.6%) were significant time cells on at least one landing ball (Fig. 1e,f and Extended Data Fig. 2a and an additional 20 examples in Extended Data Fig. 3), fulfilling the following criteria (Methods): (1) the cell exhibited a significant transient increase in firing within a specific time period after landing, which lasted for ≥3 consecutive 100-ms time bins (one-sided *t*-test versus shuffle: $P < 0.01$, Bonferroni-corrected); and (2) the firing rate was significantly enhanced within the time field in at least 40% of the trials, indicating stability (the mean number of trials per session per landing ball was 44 trials). Time cells were, thus, defined as neurons that fired transiently but reliably at a particular time after landing, while both bats were stationary (examples: Fig. 1e,f and Extended Data Figs. 2a and 3; population: Fig. 1g,h). Notably, the cells maintained temporal precision, despite the considerable trial-to-trial variation in the time spent by the bat on the balls (see vertical bands of activity in the examples in Fig. 1e,f and Extended Data Figs. 2a and 3, as compared to the diagonal end of trials). We also found high correlation of the time tuning in short trials versus long trials (Fig. 1i, main panel) and stable tuning across odd and even trials (Fig. 1i, inset). This temporal stability is in contrast to previous studies in rodents[7,10], which used a different paradigm (block design) and reported 're-timing' of time cells when the trial duration was abruptly changed. Different time cells in bat CA1 had different preferred times (Fig. 1e–g); the preferred time was defined as the time of the peak firing rate within the significant time field (Fig. 1e, bottom, and Extended Data Fig. 2a), and, as a population, the preferred times spanned the behavioral waiting time of the bats on the landing ball (median waiting time: 7.4 seconds; Fig. 1d), with an over-representation of earlier times. All the time cells exhibited only a single significant time field in each location (except one neuron that had two time fields on one of the landing balls). The width of the time field (its duration) increased with the neuron's preferred time (Extended Data Fig. 2d)—that is, the time resolution deteriorated with the passage of time, as reported also for time cells in rats[7,8,10,17], and consistent with Weber's law for the perception of interval timing[10,27]. The temporal tuning of time cells could not be explained by the occurrence of sharp-wave ripples (SWRs) (Extended Data Fig. 2g,h). Notably, time cells exhibited similar time tuning in both correct and incorrect trials (Fig. 2a,b), suggesting that the cells were not responding to the reward[28], because there was no reward on incorrect trials. This also indicates that the temporal responses of time cells were not caused by stereotypical chewing movements, because on incorrect trials the bats did not have any food reward to chew, but the neurons still maintained their time tuning. We also recorded head acceleration from the observer bat using an accelerometer, which further ruled out the possibility that stereotypical movements could underlie the time responses (Fig. 2c,d and Extended Data Fig. 4; see details in the Methods).

Notably, we found that simultaneously recorded time cells exhibited firing sequences that were very similar to the sequences found when time cells were pooled across all the recording days (Extended Data Fig. 5a–d). This demonstrates that the pooled sequences (Fig. 1g and Extended Data Fig. 5a) are reliably representing the within-day sequences (Extended Data Fig. 5b–d), indicating that the ensemble of time cells in the bat hippocampus forms internally generated firing sequences that span the behavioral epoch.

Next, we examined several additional properties of time cells. First, the time tuning was stable both within session (Fig. 1i; median $r = 0.73$) and across consecutive sessions (Extended Data Fig. 6a–c; median correlation of temporal tuning curves: $r = 0.82$; see also Extended Data Fig. 6d). Second, we examined the relation between time tuning, measured during motionless hanging, and place tuning, measured in flight. We found that time cells and place cells were largely overlapping cell populations (Fig. 1h): similar to rats, most time cells (71%) were also place cells[7,8,10]. However, there was no strong systematic relation between the location of the place field recorded in flight and the preferred time of the time field (Extended Data Fig. 7), similar to rats[8,29]. Third, time cells were found in all individual animals (Extended Data Fig. 8b–d). Fourth, we noticed a difference between the distribution of preferred times in the Start location (Fig. 1g, right) versus locations A and B (Fig. 1g, left and middle). This difference in the time representation could be due to the different physical shapes of the landing balls: whereas the start ball was ellipsoidal, landing balls A and B were spherical (Extended Data Fig. 1a,b). This difference could also be due to the behavioral task: only in the Start location was the observer landing next to another bat (the demonstrator)—a highly salient event—which could underlie the over-representation of early times in the Start location as compared to locations A and B. This explanation was supported by analysis of data from a second session, in which we removed the demonstrator bat from the room (Methods). Indeed, in this session, the distribution of preferred times in the Start location became more similar to that in locations A and B (Extended Data Fig. 6).

Two distinct neural populations: contextual and pure time cells

We next turned to the first central question of our study: Do hippocampal time cells encode context-dependent time sequences or, rather, represent time per se? To this end, we took advantage of the fact that we had three different locations in the room—that is, three spatial contexts—in all of which we measured time cells. Visual inspection of our data revealed two subsets of time cells. (1) Most of the time cells (64.7%, 123/190) were significantly time tuned only in one particular location while completely losing their time preference when the bat was in either of the other two locations (Fig. 3a: top three rows show three example cells that exhibited time tuning only in one location in the room; and Fig. 3b: population). These time cells thus encoded simultaneously time × spatial context. Indeed, across the entire population, we found very different temporal tuning curves among the three locations. When sorting the neurons by preferred times in one location, the firing sequences in the other two locations were largely lost (Fig. 3c; compare the diagonal panels to the off-diagonal panels). This indicates, again, that a large fraction of time cells encoded simultaneously time × spatial context (64.7% of all the time cells; Fig. 3b). We called these neurons 'contextual time cells'. We note that we cannot dissociate if these neurons conjunctively encoded time × spatial context or, perhaps, time × space (that is, time × spatial location), both of which are interesting possibilities. Notably, although previous studies have reported modulation of time cells in different contexts[6,7,17], it was not shown across different spatial contexts and, in particular, in different locations within the same environment. (2) The remaining time cells were significantly time tuned in more than one location. These cells tended to show a similar time preference irrespective of the bat's location (35.3% of all the time cells; Fig. 3a: fourth row shows a time cell with time tuning in locations A and B—see population analysis in Extended Data Fig. 8e,f—and the fifth row of Fig. 3a shows a time cell with time tuning in locations A and B and Start). Thus, these were 'pure' time cells, which represented elapsed time in an abstract manner, irrespective of place or context.

To examine more systematically the difference between these two populations of time cells—contextual time cells versus pure time cells—we focused on landing balls A and B, for which the task was symmetric. We separated the time cells into two non-overlapping groups: time cells that were tuned significantly on both A *and* B (Fig. 4a) and time cells that were tuned significantly on A *or* B but not both (Fig. 4b). We observed that the time sequences of cells tuned on A *and* B remained similar in both locations after sorting the cells based on their time tuning on the opposite landing ball (Fig. 4a; note the time sequences in the upper-right and lower-left panels, marked with arrows). This observation further suggested that the time tuning of cells tuned on A *and* B tended to be similar in different locations. We note that having a similar time preference in different locations is non-trivial, because,

https://doi.org/10.1038/s41593-022-01226-y

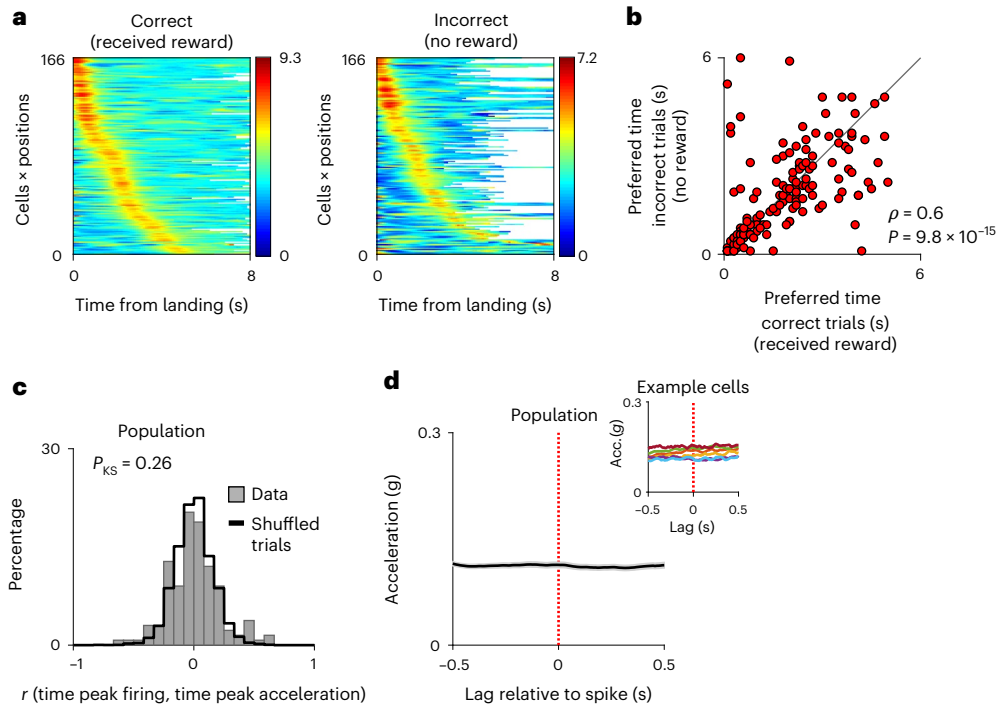

Fig. 2 | Controls for reward and movement. The firing of time cells cannot be explained by rewards or by chewing movements. **a**, Firing sequences formed by time cells in correct trials (left; trials in which bats performed correctly and received reward) and incorrect trials (right; trials in which bats did not receive reward), pooled over the two locations in the room where reward was given (balls A and B; shown are all cells × positions that had ≥10 correct and ≥10 incorrect trials: $n = 166$). *x* axis, elapsed time from the landing moment; *y* axis, temporal tuning curve of each time cell (firing rate averaged across trials). The temporal tuning curve of each neuron was *z*-scored. Color scale ranges from zero (blue) to maximal *z*-scored firing rate across all neurons (red). Time bins that did not contain enough data were colored white (this was most prevalent in tuning curves for incorrect trials, which were shorter because no reward was given, so bats tended to stay for shorter durations on the balls). Both panels were sorted by the cell's preferred time in the correct trials (that is, sorted according to left panel; note that each cell can appear here once or twice, depending on if it was tuned on ball A, B or both). **b**, Scatter plot of preferred time in correct trials, when bats received reward, versus preferred time in incorrect trials, when bats did not receive reward. Dots: cells × positions ($n = 166$: same cells × positions as in **a**); gray diagonal line: identity line. Note high correlation between preferred time in correct, rewarded trials and incorrect, non-rewarded trials (Spearman correlation $\rho = 0.6$; $P = 9.8 \times 10^{-15}$; two-sided test). **c**,**d**, The firing of time cells cannot be explained by fine movements (measured using an accelerometer; we included here $n = 133$ time cells (cells × positions), which are all the time cells for which an accelerometer was recorded). **c**, Distribution of Pearson correlations across trials between the time of peak firing in each trial and the time of per-trial peak acceleration within the time field (gray bars). This distribution is indistinguishable from the shuffle distribution (black line; shuffle distribution shows the correlation for each time cell between time of peak firing in trial *i* and time of peak acceleration in trial *j*, for $i \neq j$; two-sided Kolmogorov–Smirnov (KS) test between data and shuffle: $P = 0.26$; $n = 133$ cells). **d**, Spike-triggered average of accelerometer signal in each trial, averaged across trials and across all time cells (acceleration shown in units of Earth acceleration, *g*; gray shading, mean ± s.e.m.; $n = 133$ cells × positions). Inset: examples of spike-triggered accelerometer signal ('Acc.') from individual cells. Additional controls for movement are shown in Extended Data Fig. 4.

here, the distinction between contextual and pure time cells was based on whether a cell is tuned on A *or* B versus whether it is tuned on both A *and* B—and, a priori, based on this selection criterion, there is no reason that a time cell active in both locations should have a similar time preference, as exhibited here by the pure time cells. Therefore, the conserved time tuning of pure time cells is quite surprising.

To test this further, we compared the preferred times of cells tuned on A *and* B in the different locations. First, we found that 61.4% (27/44) of the cells tuned on A *and* B had preferred time difference <1 second (Extended Data Fig. 8e, top). This percentage was 2–3-fold higher than expected by chance (chance level could be quantified in two ways: (1) 22.2% = the gray area in Extended Data Fig. 8e, top, divided by the total area; or (2) 35.2% (333/946 shuffles), when calculated using cell shuffling of cells tuned on A *and* B; Extended Data Fig. 8e, bottom). Second, we found that the distribution of ΔT (preferred time on A − preferred time on B) for cells tuned on A *and* B was centered around zero, with a prominent narrow peak (Fig. 4c, pink). Furthermore, this peak was significantly narrower compared to the distribution for cells tuned on A *or* B (Fig. 4c, green) (non-parametric *F*-test (Ansari–Bradley test) for equality of variances $P = 6.8 \times 10^{-4}$), suggesting that cells tuned on A *or* B did *not* have a similar but weak time tuning in their non-significant location. The distribution for cells tuned on A *and* B (pink) was also significantly narrower compared to three different shuffles (comparisons were done via non-parametric *F*-test (Ansari–Bradley test) for equality of variances). (1) A *and* B versus cell shuffling of cells tuned on A *and* B (Fig. 4c, pink versus black dotted line: $P = 3.8 \times 10^{-2}$; for the cell shuffling, we computed ΔT between cell *i* at location A and cell *j* at location B, for $i \neq j$). (2) A *and* B versus cell shuffling of all cells (Fig. 4c, pink versus red dotted line: $P = 5.9 \times 10^{-5}$). (3) A *and* B versus cell shuffling of cells tuned on A and cells tuned on B but not tuned on both (Fig. 4c, pink versus blue dotted line: $P = 1.02 \times 10^{-3}$). The highly significant narrowness of the ΔT distribution for pure time cells as compared to three different shuffles emphasizes the robustness of our results—namely, that pure time cells have similar time tuning in both locations. Similar time tuning was found also for neurons that were significant time cells on all three balls: A, B and start (Fig. 4d; non-parametric *F*-test versus shuffle, $P = 4.2 \times 10^{-3}$). Furthermore, pure time cells were also stably tuned across sessions (Extended Data Fig. 8h,i). Together, these results suggests that the group of cells tuned on A *and* B contains a large fraction of neurons that are pure time cells, encoding elapsed time irrespective of location and context.

https://doi.org/10.1038/s41593-022-01226-y

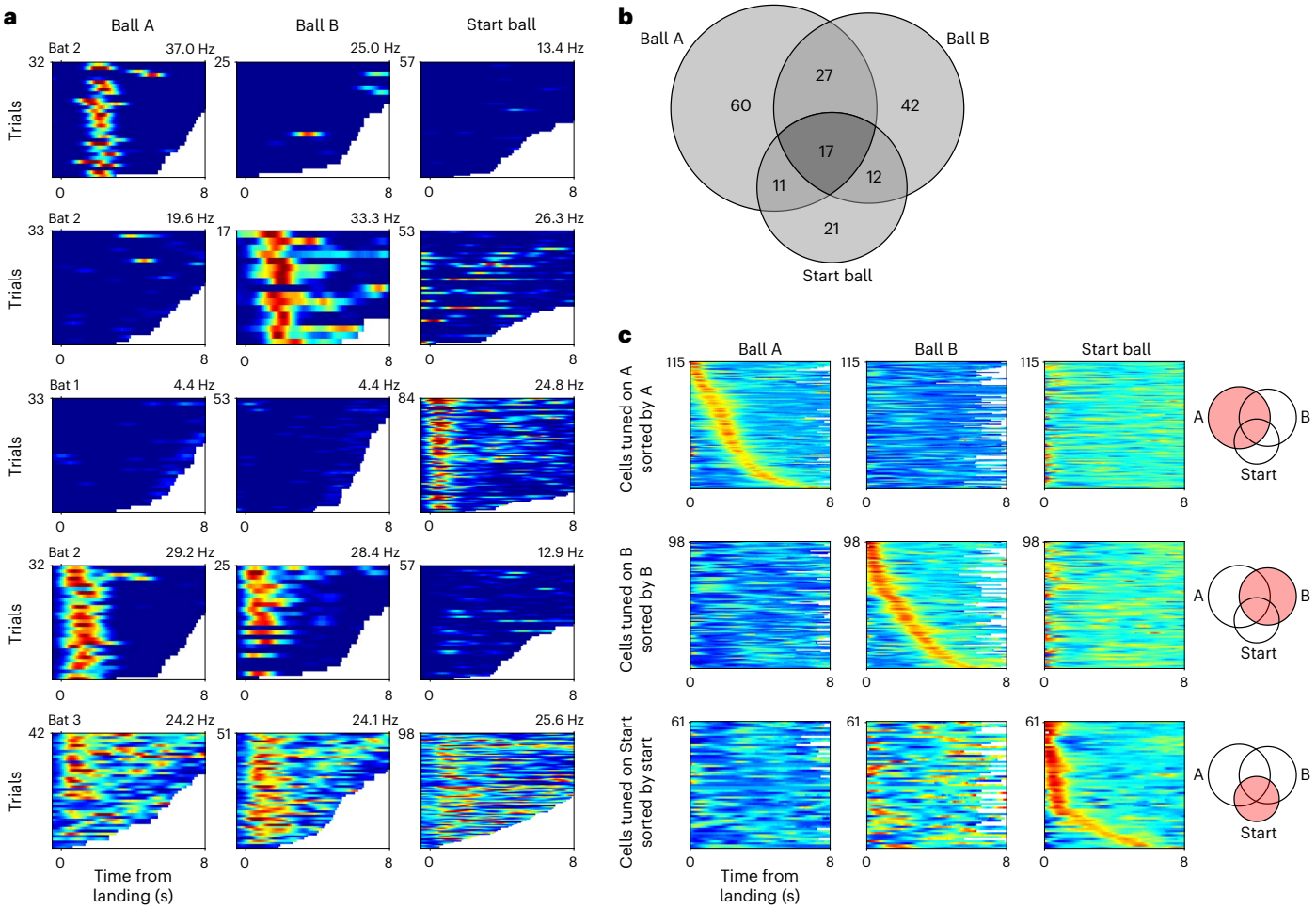

Fig. 3 | Comparing time tuning at different locations. a, Five example time cells (rows) that were active in only one location (balls A, B or Start: top three neurons), in two locations (4th neuron) or in all three locations (5th neuron), plotted as in Fig. 1f. **b**, Venn diagram: total numbers of significant time cells in the three locations. **c**, Firing sequences in each of the three locations in the room (columns), plotted separately for the population of time cells that were significantly tuned in each of the locations (rows); each panel is plotted as in Fig. 1g. The neurons in each row of the panels are sorted by their preferred time of firing in location A (top row), B (middle row) or Start (bottom row); icons of Venn diagrams depict the group of time cells plotted in each row. Note that the firing sequence of time cells in one location was disrupted in the other locations (compare across columns)—that is, most neurons encoded simultaneously time × spatial context (or, alternatively, time × space).

By contrast, for the group of cells tuned on A *or* B, the time sequence was completely lost between the two locations (Fig. 4b; see also Fig. 4c: no difference between the A *or* B group (green) and the shuffle for all cells: non-parametric *F*-test, $P = 0.7$). This demonstrates that this group of neurons encoded simultaneously time × spatial context—that is, they were contextual time cells.

Next, we examined whether these two groups of time cells belong to two distinct populations of cells, or do they form a continuum? To this end, we computed for each group the distribution of Pearson correlations between the temporal tuning curves of each cell in location A versus location B and compared it to three control shuffle distributions (Fig. 4e; for the cell shuffling, we computed the correlations between cell i at location A and cell j at location B, for $i \neq j$). The distribution of correlations for the cells tuned on A *or* B was symmetric around zero (Fig. 4e, green) and was statistically indistinguishable from the three shuffle distributions (Fig. 4e; same three shuffles as in Fig. 4c; Kolmogorov–Smirnov test: $P = 0.274$, $P = 0.10$ and $P = 0.24$ for the three shuffles; Wilcoxon rank-sum test: $P = 0.275$, $P = 0.90$ and $P = 0.48$). By contrast, the distribution of correlations for cells tuned on A *and* B was significantly skewed to the right (Fig. 4e, pink) and was significantly very different from the three shuffle distributions and from the A *or* B distribution (Kolmogorov–Smirnov test: $P = 4.5 \times 10^{-5}$, $P = 2.8 \times 10^{-7}$, $P = 2 \times 10^{-6}$ and $P = 2.1 \times 10^{-5}$; Wilcoxon rank-sum test: $P = 2.8 \times 10^{-5}$, $P = 8.0 \times 10^{-7}$, $P = 2.5 \times 10^{-6}$ and $P = 8.6 \times 10^{-5}$). The clear separation of the distributions suggests that these are two distinct groups of cells and not a continuum (Fig. 4e, compare green-colored and pink-colored distributions; we note that the firing rate characteristics did not differ substantially between the two groups; Extended Data Fig. 5h). The distinctness of the two populations was supported also by four further analyses. (1) A statistical test demonstrated that these correlations were not distributed unimodally but, in fact, had a dip (Hartigan's dip test for unimodality, pooling together the pink and green distributions of Pearson correlations in Fig. 4e: $P = 0.015$; see inset for the pooled distribution—the red arrow in the inset shows the dip). (2) As shown above, we found a distinct dissimilarity among these groups of cells in terms of the distributions of time differences ($\Delta T_{\text{pref-time}}$) between balls A and B: the A *and* B group exhibited a narrow distribution of time differences (Fig. 4c, pink), whereas much wider distributions were exhibited by the A *or* B group and by additional three distributions of cell shuffling (Fig. 4c). (3) The identity of pure time cells and contextual time cells was stable across recording sessions (χ^2 test: $P = 3.8 \times 10^{-5}$), which is consistent with the existence of two independent populations. (4) To test if the fraction of pure time cells was significantly higher than expected from the conjoint probabilities for neurons to be time cells

https://doi.org/10.1038/s41593-022-01226-y

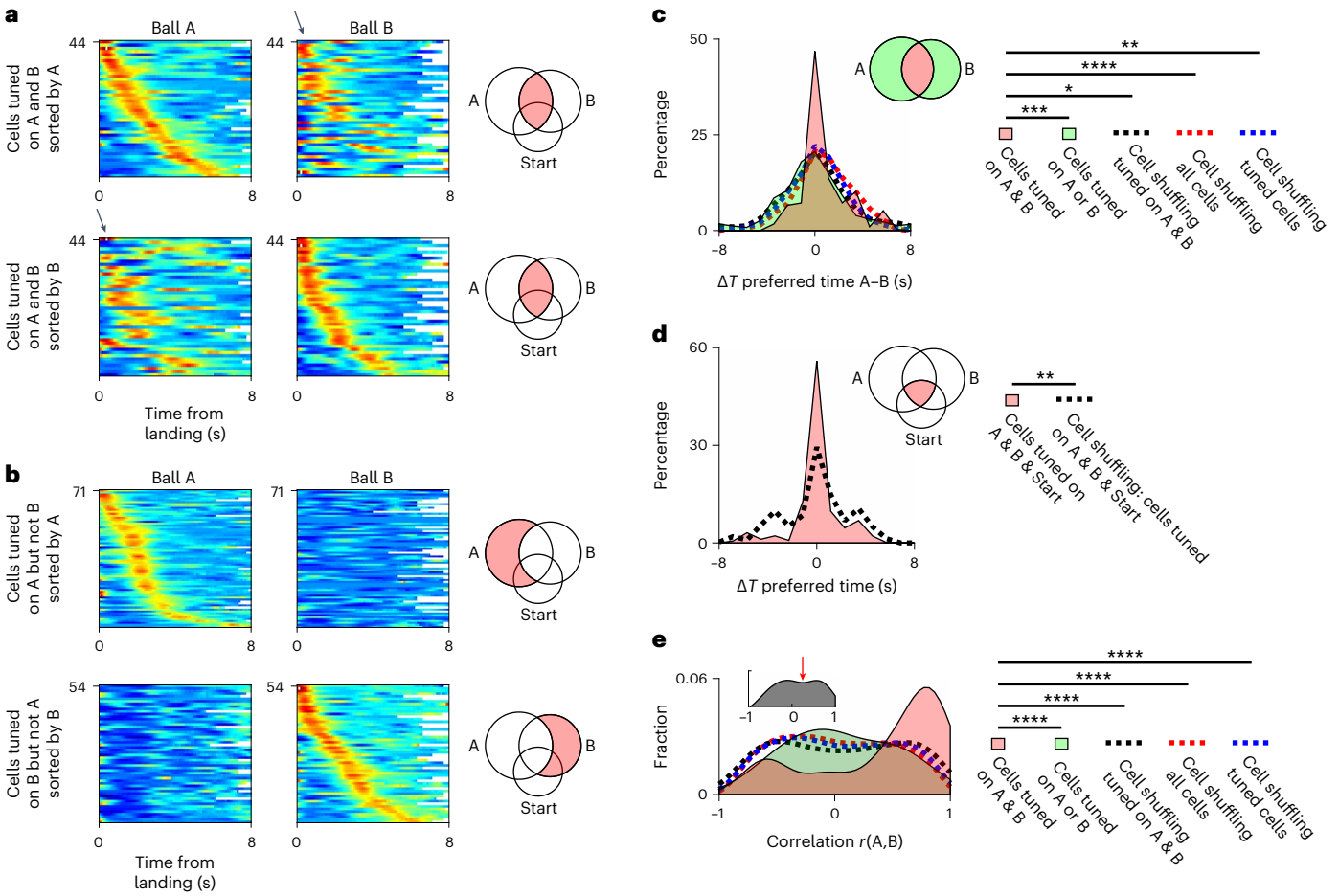

Fig. 4 | Two distinct populations of hippocampal time cells: contextual time cells and pure time cells. a, Firing sequences for the subpopulation of time cells significantly tuned in both locations A and B ($n = 44$ cells), plotted for locations A (left) and B (right) and sorted by preferred time of firing in A (top) or B (bottom). Note the similarity of firing sequences in both locations (see 'halo' when comparing across columns—marked with black arrows). **b**, Same as **a**, but here each row depicts the firing sequences of time cells tuned in either location A or B ($n = 125$ cells; see Venn icons). Note the complete disruption of firing sequences in the non-preferred locations (compare columns; note the absence of the 'halo' seen in **a**). **a** and **b** are plotted as in Fig. 3c. **c,** Distributions (kernel density plots) of the differences in preferred time (ΔT) between balls A and B, for all time cell pairs belonging either to the group of time cells tuned on A *and* B (pure time cells, pink) or the group of time cells tuned only in one of the locations, A *or* B (contextual time cells, green; here, the difference ΔT was calculated between preferred time on the tuned ball and time of maximum firing rate on the other ball, as these cells were tuned only on one ball). Three types of shuffles are shown, all showing ΔT for cell i at location A minus cell j at location B, for $i \neq j$ (cell shuffling). (1) Dotted black line: shuffle for the population of cells tuned on both A and B (946 shuffles from 44 cells)—that is, where the same cell was tuned on both. (2) Dotted red line: shuffle for all cells (14,196 shuffles from 169 cells). (3) Dotted blue line: shuffle distribution of ΔT between preferred times of tuned cells (where cell i was significantly tuned on ball A and cell j was significantly tuned on ball B (but not tuned on both), for $i \neq j$; 5,577 shuffles from 213 responses). Note the distribution of ΔT for time cells tuned on A *and* B (pink) was centered around zero, with a prominent peak, and was significantly narrower than the distribution of time cells tuned on A *or* B (green) (two-sided non-parametric F-test (Ansari–Bradley test) for equality of variances: $P = 6.8 \times 10^{-4}$); and it was also significantly narrower than the three shuffle distributions (two-sided non-parametric F-test of the pink distribution versus the three shuffles: $P = 3.8 \times 10^{-2}$, $P = 5.9 \times 10^{-5}$ and $P = 1.02 \times 10^{-3}$). **d**, Distributions (kernel density plots) of differences in preferred time (ΔT) among balls A, B or start, for all pure time cells that were significantly tuned on A and B and start (pink; $n = 17$ cells). Time differences ΔT for each cell were pooled across the three pairs of balls. Dotted black line: shuffle distribution of ΔT for all cells. Data distribution was significantly narrower than shuffle (non-parametric F-test: $P = 4.2 \times 10^{-3}$). **e**, Distributions of Pearson correlations between temporal tuning curves on ball A versus ball B for all pairs of time cells tuned on A *and* B (pink: the cells in **a**) and for pairs of time cells tuned on A *or* B (green: the cells in **b**) as well as for shuffled cell pairs (black, red and blue dotted lines: three cell-shuffling populations, same as in **c**). Inset: distribution of Pearson correlations for all time cells; red arrow marks the dip in the distribution, indicating bimodality (Hartigan's dip test for unimodality: $P = 0.015$).

in one of the locations separately, we used a binomial test, where the chance proportion of time cells expected to be tuned in both A and B, or in A and B and start, is equal to the multiplication of the observed probabilities on each landing ball separately (p(ball A) = 115/391; p(ball B) = 98/391; p(start ball) = 61/391). The observed fraction of pure time cells was significantly higher than expected by chance (binomial test: $P = 0.0037$ for the 44 pure time cells tuned on A *and* B and $P = 4.3 \times 10^{-6}$ for the 17 pure time cells tuned on all three locations). These results thus reveal the existence of two distinct populations of time cells: one population that encodes elapsed time per se and another population that encodes time × spatial context. Interestingly, despite the functional bimodality, these two populations were anatomically intermixed in dorsal CA1 (in 75% of the tetrodes, we recorded both types of time cells on the same tetrode).

Finally, Bayesian maximum likelihood decoding revealed that each of these populations of time cells represented time very precisely, with decoding error <0.6 seconds over the entire temporal range of 8 seconds (Extended Data Fig. 5e; see also Extended Data Fig. 5f, showing 'cross-decoding' of time using only pure time cells with ΔT difference of <1 second in preferred time; Methods).

Time cells for other individuals

Finally, we asked whether there are time cells in the hippocampus that encode elapsed time from the landing moment of the other bat (demonstrator; Fig. 5a). Surprisingly, we found time cells for the other bat, with significant and reliable transient firing at a specific time relative to the landing moment of the other bat (examples: Fig. 5b; see additional 12 examples in Extended Data Fig. 9c; population: Fig. 5c–g; we used here the same criteria as used for defining time cells for self). The firing of these time cells for the other could not be explained by self movements of the observer bat, because the observer was motionless on the start ball (Fig. 2c,d and Extended Data Fig. 4). It could also not be explained as late firing of self time cells aligned to self (observer) landing, because the stationary delay times on the balls were highly variable (Fig. 1d). A total of 56 out of the 391 recorded neurons (14.3%) were significant time cells for the other. The firing rates of time cells for the other were lower than time cells for self (peak firing rate: self: 6.36 ± 4.40 Hz, mean ± s.d.; other: 4.71 ± 3.00 Hz; *t*-test: $P = 0.011$), but, notably, the temporal responses of time cells for the other bat were very stable (Fig. 5h; median stability: $r = 0.65$). Similarly to self time cells, the time cells for the other showed the following. (1) Increased width (duration) of their time field as a function of the neuron's preferred time (Extended Data Fig. 9a)—that is, the time resolution deteriorated with the passage of time. (2) At the population level, these time cells formed internally generated firing sequences for the other (Fig. 5c, panels on the diagonal), which spanned the entire waiting time of the other bat (Fig. 5d; median waiting time, 5.7 seconds). Furthermore, simultaneously recorded time cells for the other exhibited firing sequences akin to the pooled data (Extended Data Fig. 9b), suggesting that time cells for the other bat form internally generated firing sequences that span the entire behavioral epoch. (3) The overall distribution of preferred times was very similar for the time cells for self and other (Fig. 5f,g; Kolmogorov–Smirnov test: $P = 0.12$). Many of the time cells for the other bat were also self time cells for the observer bat (Fig. 5i; $n = 38$); interestingly, these neurons generally exhibited different preferred times for self and other (Fig. 5j; Kolmogorov–Smirnov test compared to cell shuffling: $P = 0.63$; $n = 38$). Some of the time cells for the other bat were also social place cells[24,25]—that is, encoded the location of the other bat when it was flying (Fig. 5k).

One caveat to the social nature of the time cells for the other bat is that we could not analyze time cells for objects and, thus, could not discern whether the responses are truly social (in session 2, where we replaced the demonstrator bat with an object, we could not analyze social time cells because the object was kept for only brief moments on the landing ball; Methods). It remains to be determined whether social time cells would be recorded in bats learning by watching the movements of an object instead of a bat.

To test whether the time cells for the other bat encode pure time or time × spatial context, we repeated some of the same analyses as for the self time cells. First, we found evidence for neurons encoding time × spatial context for the other bat ('contextual time cells for the other'). Most neurons (42/56, 75%) were significantly time tuned in only one of the locations (Fig. 5c,e). Second, we found evidence also for pure time cells for the other bat. Twelve cells were tuned on both A *and* B (21.4% of time cells for the other), and, notably, the distribution of time difference ΔT for these time cells was centered around zero, with a prominent peak (Fig. 5l, pink), and was significantly narrower than both the distribution of time cells tuned on A *or* B (green) and the shuffle distributions (dotted lines) (non-parametric *F*-test: comparing A *and* B to A *or* B: $P = 4.7 \times 10^{-4}$; comparing A *and* B to the three shuffle distributions (similar shuffles to Fig. 4c): $P = 2.5 \times 10^{-4}$, $P = 1.2 \times 10^{-5}$ and $P = 0.11$ for the three types of shuffles—shuffle of cells tuned on A and cells tuned on B but not tuned on both (blue dotted line); shuffle of all cells (red dotted line); and shuffle of cells tuned on A *and* B (black dotted line)). By contrast, there was no significant difference in the distribution width for the time cells tuned on A *or* B (green) versus the shuffle distribution for all cells (red dotted line; $P = 0.08$). The narrow distribution of ΔT for the 12 time cells that were tuned in both locations A *and* B (pink) may suggest that these time cells for the other had the same time preference, regardless of the location—that is, were 'pure time cells for the other'. Together, these results indicate that time cells for the other encoded elapsed time for the other bat, via internally generated firing sequences, with some of these neurons being contextual time cells, simultaneously encoding time × spatial context for the other bat, whereas other neurons were pure time cells for the other.

Discussion

In this study, we found time cells in bats that were stationary on resting platforms. We identified two distinct populations of self time cells. Contextual time cells were highly selective to the spatial context and could, thus, be involved in encoding episodic information (what, where and when). Pure time cells exhibited robust temporal tuning that was invariant to location and context and could, thus, represent elapsed time per se, which, we propose, may support the perception of interval timing. For both types of time cells, the encoding of elapsed time was robust and unaffected by trial duration—that is, their time tuning did not show re-timing for different trial durations. We ruled out reward delivery times as explaining the firing of time cells. Nevertheless, it is still possible that the firing of time cells is explained by the bat's

Fig. 5 | Time cells for the other bat. a, The three conditions that were used to analyze and align time cells for the other bat. **b**, Seven example time cells for the other bat (demonstrator): neurons that were recorded in hippocampal area CA1 of the observer bat, and which showed significant and reliable firing at a preferred time moment after the landing of the other bat, plotted as in Fig. 1f. See additional 12 examples in Extended Data Fig. 9c. **c**, Firing sequences in each of the three locations in the room (columns), plotted separately for the populations of time cells for the other bat that were significantly tuned in each of the three locations (rows), plotted as in Fig. 3c. **d**, Distribution of trial durations for the demonstrator bat (that is, waiting times of demonstrator bat on the landing balls); the median trial duration was 5.7 seconds (blue arrowhead). **e**, Venn diagram: total numbers of time cells for the other bat in the three locations. **f**,**g**, Similar distributions of preferred times for self and other. **f**, Cumulative distribution of preferred times for the time cells for self (red) and time cells for the other bat (blue). *y* axis normalized to total number of recorded cells × positions. Note the high similarity of the two distributions (two-sided Kolmogorov–Smirnov test: $P = 0.12$). **g**, The ensemble activity of time cells for the other bat (bottom) spanned a similar time interval as the time cells for self (top); shown are significant temporal responses for all three locations (cells × positions). Each panel was plotted as in Fig. 1g. **h**, Stability of the temporal tuning curve for each time cell for the other bat (cells × positions). Shown is the distribution of Pearson correlations between the cell's temporal tuning curve in short trials (duration < median trial duration) versus its temporal tuning curve in long trials (≥ median trial duration; median value of correlations: $r = 0.65$). **i**, Total numbers of time cells for the other bat and time cells for self. Cell counts here refer to neurons, unlike **g** where numbers represent cells × positions. **j**, Distributions of ΔT between preferred times for self and other, for the 38 time cells that were tuned for both self and other (green); this distribution is statistically indistinguishable from shuffled cell pairs where ΔT was calculated between the preferred time for self in cell i and preferred time for other in cell j, for $i \neq j$ (same $n = 38$ cells; two-sided Kolmogorov–Smirnov (KS) test: $P = 0.63$). **k**, Total numbers of time cells for the other bat and of social place cells. **l**, Distributions (kernel density plots) of the differences in preferred time (ΔT) between balls A and B, for all the time cells for the other bat that belonged either to the group of time cells tuned on A *and* B (pure time cells for the other; pink) or to the group of time cells tuned only in one of the locations, A *or* B (contextual time cells for the other; green) (pink versus green: two-sided non-parametric *F*-test (Ansari–Bradley test) for equality of variances: $P = 4.7 \times 10^{-4}$). Dotted lines: three shuffle distributions, plotted as in Fig. 4c (two-sided non-parametric *F*-test of pink distribution versus the three shuffles: $P = 0.11$, $P = 1.2 \times 10^{-5}$ and $P = 2.5 \times 10^{-4}$). NS, not significant.

https://doi.org/10.1038/s41593-022-01226-y

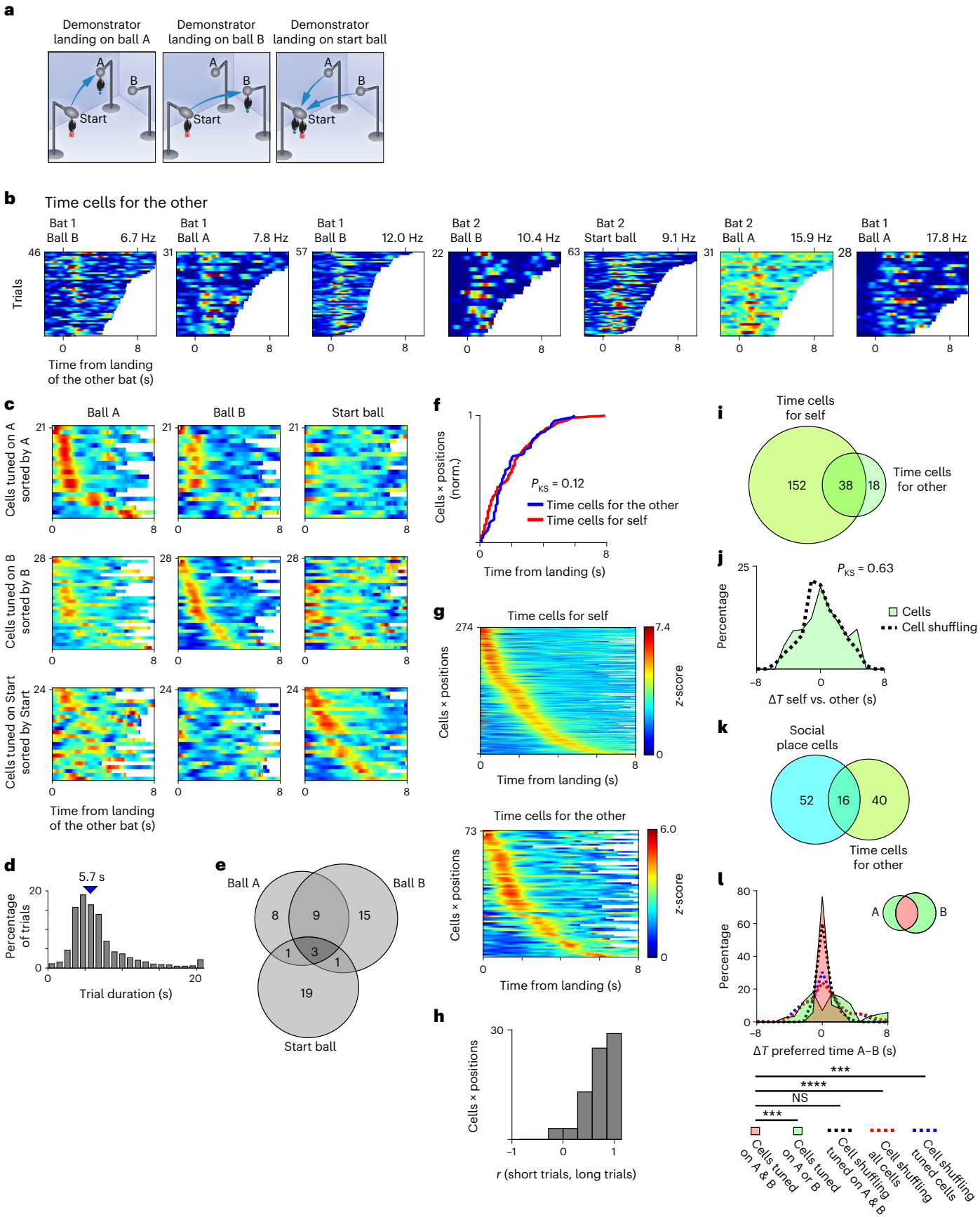

expected reward delivery time; under this interpretation, the trigger for the time sequence is the time of reward expectation rather than the time of landing per se. This seems, however, less likely because, on incorrect trials, there was no reward—hence, the bat most likely did not expect any reward on these trials—and yet the time cells fired in a very similar manner as on correct, rewarded trials (Fig. 2a,b). Nevertheless, future work should be done to examine more specifically whether expectation of reward (rather than actual reward delivery) triggers firing of time cells.

Our study revealed four main findings. (1) First, to our knowledge, this is the first report on two distinct bimodal populations of time cells (in this case, pure and contextual time cells). (2) Second, this is the first study that found different time coding by time cells in different locations within the same environment. Previous studies reported on time cells in completely different spatial contexts[12] but not in different locations within the same environment. (3) Third, the intriguing pure time cells, which encoded time per se, not linked to any behavioral sequence or context, provide, to our knowledge, the first example, in any species, of neurons that purely encode elapsed time. (4) Fourth, another surprising result is the finding of cells encoding elapsed time for another individual; such cells were not reported to date. Previous studies have reported internally generated firing sequences in a number of brain regions, and these sequences were shown to represent a variety of cognitive variables relative to the behavior of the self[6,30–33]. However, the present work is the first to show internally generated sequences relative to the behavior of *another* agent, in a social context. These internally generated sequences (i) may represent elapsed time for the other or (ii) may represent sequential activity of self time cells that was triggered by an external cue or sensory stimulus—such as the sight or sound of the other bat's landing or by the increased rate of the other's biosonar signals as it landed[34]. (iii) Or, perhaps, these internally generated sequences represent memory of self landing that was retrieved upon the other bat's landing. Although we cannot dissociate these possibilities, in all these cases the trigger for the sequence was an event 'out there' rather than the behavior of the implanted bat itself. Importantly, to our knowledge, this is the first demonstration of time cell sequences in the mammalian hippocampus that are triggered by an external action of another conspecific and, thus, constitute an explicit temporal representation of elapsed time for another individual. This also hints at the possible existence of two reference frames for time: one reference frame that is triggered by the animal's own actions (self time cells) and another reference frame that is triggered by external events (other's time cells). A neural representation of elapsed time for others may be crucial for the survival and reproduction of social animals, as any social interactions require temporal coordination. Furthermore, it is possible that shared mechanisms exist for remembering events that happened to oneself (that is, episodic memory) and events that happened to other individuals. We, therefore, speculate that the coding of time × spatial context for self and other, described here, could be part of a rudimentary brain mechanism for representing episodic memories for self and others.

Online content

Any methods, additional references, Nature Portfolio reporting summaries, source data, extended data, supplementary information, acknowledgements, peer review information; details of author contributions and competing interests; and statements of data and code availability are available at https://doi.org/10.1038/s41593-022-01226-y.

References

1. O'Keefe, J. & Nadel, L. *The Hippocampus as a Cognitive Map* (Oxford University Press, 1978).
2. Scoville, W. B. & Milner, B. Loss of recent memory after bilateral hippocampal lesions. *J. Neurol. Neurosurg. Psychiatry* **20**, 11–21 (1957).
3. Tulving, E. *Elements of Episodic Memory* (Oxford University Press, 1983).
4. Squire, L. R. Memory and the hippocampus: a synthesis from findings with rats, monkeys, and humans. *Psychol. Rev.* **99**, 195–231 (1992).
5. Eichenbaum, H. & Cohen, N. J. Can we reconcile the declarative memory and spatial navigation views on hippocampal function? *Neuron* **83**, 764–770 (2014).
6. Pastalkova, E., Itskov, V., Amarasingham, A. & Buzsáki, G. Internally generated cell assembly sequences in the rat hippocampus. *Science* **321**, 1322–1327 (2008).
7. MacDonald, C. J., Lepage, K. Q., Eden, U. T. & Eichenbaum, H. Hippocampal 'time cells' bridge the gap in memory for discontiguous events. *Neuron* **71**, 737–749 (2011).
8. Kraus, B. J., Robinson, R. J. 2nd, White, J. A., Eichenbaum, H. & Hasselmo, M. E. Hippocampal 'time cells': time versus path integration. *Neuron* **78**, 1090–1101 (2013).
9. Modi, M. N., Dhawale, A. K. & Bhalla, U. S. CA1 cell activity sequences emerge after reorganization of network correlation structure during associative learning. *eLife* **3**, e01982 (2014).
10. Eichenbaum, H. Time cells in the hippocampus: a new dimension for mapping memories. *Nat. Rev. Neurosci.* **15**, 732–744 (2014).
11. Kraus, B. J. et al. During running in place, grid cells integrate elapsed time and distance run. *Neuron* **88**, 578–589 (2015).
12. Heys, J. G. & Dombeck, D. A. Evidence for a subcircuit in medial entorhinal cortex representing elapsed time during immobility. *Nat. Neurosci.* **21**, 1574–1582 (2018).
13. Mau, W. et al. The same hippocampal CA1 population simultaneously codes temporal information over multiple timescales. *Curr. Biol.* **28**, 1499–1508 (2018).
14. Heys, J. G., Wu, Z., Allegra Mascaro, A. L. & Dombeck, D. A. Inactivation of the medial entorhinal cortex selectively disrupts learning of interval timing. *Cell Rep.* **32**, 108163 (2020).
15. Shimbo, A., Izawa, E. I. & Fujisawa, S. Scalable representation of time in the hippocampus. *Sci. Adv.* **7**, eabd7013 (2021).
16. Taxidis, J. et al. Differential emergence and stability of sensory and temporal representations in context-specific hippocampal sequences. *Neuron* **108**, 984–998 (2020).
17. MacDonald, C. J., Carrow, S., Place, R. & Eichenbaum, H. Distinct hippocampal time cell sequences represent odor memories in immobilized rats. *J. Neurosci.* **33**, 14607–14616 (2013).
18. Umbach, G. et al. Time cells in the human hippocampus and entorhinal cortex support episodic memory. *Proc. Natl Acad. Sci. USA* **117**, 28463–28474 (2020).
19. O'Keefe, J. & Dostrovsky, J. The hippocampus as a spatial map. Preliminary evidence from unit activity in the freely-moving rat. *Brain Res.* **34**, 171–175 (1971).
20. Wilson, M. A. & McNaughton, B. L. Dynamics of the hippocampal ensemble code for space. *Science* **261**, 1055–1058 (1993).
21. Leutgeb, S. et al. Independent codes for spatial and episodic memory in hippocampal neuronal ensembles. *Science* **309**, 619–623 (2005).
22. Ulanovsky, N. & Moss, C. F. Hippocampal cellular and network activity in freely moving echolocating bats. *Nat. Neurosci.* **10**, 224–233 (2007).
23. Kay, K. et al. A hippocampal network for spatial coding during immobility and sleep. *Nature* **531**, 185–190 (2016).
24. Danjo, T., Toyoizumi, T. & Fujisawa, S. Spatial representations of self and other in the hippocampus. *Science* **359**, 213–218 (2018).
25. Omer, D. B., Maimon, S. R., Las, L. & Ulanovsky, N. Social place-cells in the bat hippocampus. *Science* **359**, 218–224 (2018).
26. Stangl, M. et al. Boundary-anchored neural mechanisms of location-encoding for self and others. *Nature* **589**, 420–425 (2021).

27. Gibbon, J., Malapani, C., Dale, C. L. & Gallistel, C. Toward a neurobiology of temporal cognition: advances and challenges. *Curr. Opin. Neurobiol.* **7**, 170–184 (1997).
28. Gauthier, J. L. & Tank, D. W. A dedicated population for reward coding in the hippocampus. *Neuron* **99**, 179–193 (2018).
29. Wang, Y., Romani, S., Lustig, B., Leonardo, A. & Pastalkova, E. Theta sequences are essential for internally generated hippocampal firing fields. *Nat. Neurosci.* **18**, 282–288 (2015).
30. Harvey, C. D., Coen, P. & Tank, D. W. Choice-specific sequences in parietal cortex during a virtual-navigation decision task. *Nature* **484**, 62–68 (2012).
31. Tingley, D. et al. Task-phase-specific dynamics of basal forebrain neuronal ensembles. *Front. Syst. Neurosci.* **8**, 174 (2014).
32. Aronov, D., Nevers, R. & Tank, D. W. Mapping of a non-spatial dimension by the hippocampal–entorhinal circuit. *Nature* **543**, 719–722 (2017).
33. Buzsáki, G. & Tingley, D. Space and time: the hippocampus as a sequence generator. *Trends Cogn. Sci.* **22**, 853–869 (2018).
34. Yovel, Y., Falk, B., Moss, C. F. & Ulanovsky, N. Optimal localization by pointing off axis. *Science* **327**, 701–704 (2010).

Methods

Subjects and behavioral setup

We collected data from four pairs of adult male Egyptian fruit bats (*Rousettus aegyptiacus*; eight bats in total, weights 160–179 g). Each pair consisted of an 'observer bat' and a 'demonstrator bat', which were trained to fly in a flight room (2.35 × 2.69 × 2.56 m; Fig. 1a). The pair of bats were not siblings but were cagemates that were housed together for several weeks to months before the start of the experiment and were, thus, highly familiar with each other. The demonstrator bat in each pair was usually the more dominant male, and it was a highly trained animal—both of which played an important role in the task[25]. The observer bat in each pair was always the bat that, after training, was implanted with a microdrive for electrophysiological recordings. The flight data from this experiment were published elsewhere[25]; here we report on unpublished data, taken only from stationary epochs, when both bats were hanging motionlessly on the balls and neither of them was flying (Fig. 1b,c and Extended Data Figs. 1 and 4). The room was dimly illuminated (illuminance level: 3 lux). We positioned three landing balls in three different locations inside the room: 'Start', 'A' and 'B' locations (Fig. 1a and Extended Data Fig. 1a,b). Landing balls A and B were elevated spheres (12-cm diameter; height above floor: 115 cm), positioned at the far corners of one side of the room; the start ball was an elevated ellipsoid (12 × 30 cm, height above floor: 150 cm) and was positioned next to the wall that was opposite to balls A and B (Fig. 1a). The linear distance between the start ball and landing balls A and B was ~170 cm. The balls always remained in the same locations, across all experimental days and all bats.

We conducted three kinds of behavioral sessions[25], but, for this study, we analyzed only session 1 throughout the paper as well as session 2 in Extended Data Fig. 6 and Extended Data Fig. 8g–i. Session 1, the 'observer–demonstrator' session, was conducted in all four pairs of bats. The demonstrator bat was trained to fly roughly randomly from the start ball to ball A or B. It was then rewarded by the experimenter, regardless of its flight choice. The demonstrator bat then flew back to the start ball, on its own volition. The observer bat (from whose hippocampus we recorded; see below) was trained to remain stationary and wait for the demonstrator to return to the start ball; and after its return, the observer was trained to imitate the demonstrator's ball choice—that is, the observer had to fly to the same ball as the demonstrator (Extended Data Fig. 1a–c). On correct trials, the experimenter manually rewarded the observer bat for correct performance with ~0.05 ml of banana mash; all the correct trials were rewarded; no reward was given on incorrect trials. The reward was given only on balls A and B, not on the start ball, and it was always given immediately after landing or soon thereafter; this was the case for both the observer and the demonstrator. In all the analyses in this study, we always analyzed data from correct and incorrect trials pooled together—except Fig. 2a,b, where we separated them and explicitly compared neuronal responses on correct versus incorrect trials. The time of reward delivery by the experimenter (as extracted from the video) was highly variable and did not affect the firing of time cells (Extended Data Fig. 4g–i).

We defined the onset of each trial as the landing moment of one of the bats on one of the landing balls (see 'Estimating the locations of the bats' below). For 'self time cells' (see 'Definition of time cells' below), the trial onset was defined as the landing moment of the observer bat; and, for 'time cells for the other', the trial onset was defined as the landing moment of the demonstrator bat. We defined the trial end as follows (Fig. 1c and Extended Data Fig. 1). For self time cells: when the observer bat landed on balls A or B, we defined the trial end as the takeoff moment of the observer back to the start ball; when the observer bat landed on the start ball, we defined the trial end as the takeoff moment of the demonstrator bat (the other bat) away from the start ball. Likewise, for time cells for the other: when the demonstrator bat landed on balls A or B, we defined the trial end as the takeoff moment of the demonstrator back to the start ball; when the demonstrator bat landed on the start ball, we defined the trial end as the takeoff moment of the observer (the implanted bat) away from the start ball. Note that, in all of these cases, both bats were stationary on one of the landing balls during the entire trial (Fig. 1c and Extended Data Fig. 1b,c). Note also that the trial duration varied substantially from trial to trial, because the bats took off on their own volition (Figs. 1d and 5d).

At the end of session 1, we removed the demonstrator bat from the flight room. Session 2 was conducted in two of the four pairs of bats and was analyzed only in Extended Data Figs. 6 and 8g–i. In this session, which started immediately after session 1, we replaced the demonstrator bat with a plastic object ('informative object'). We mounted the object on a thin metal rod and manually moved it from the start ball, roughly randomly, to either ball A or ball B and then back. We trained the observer to follow the same set of behavioral rules as in the 'observer–demonstrator' session 1, but, this time, we trained it to imitate the object's ball 'choices' instead of the ball choices of the demonstrator bat. The set of all behavioral sessions was flanked by sleep sessions (~5–10 minutes each).

After training, the observer bat in each pair was implanted with a four-tetrode microdrive for electrophysiological recordings. We recorded the neuronal activity continuously throughout all the sessions, including the sleep sessions, to facilitate spike sorting and to assess the stability of the recorded neurons.

Surgery and recording techniques

The Institutional Animal Care and Use Committee of the Weizmann Institute of Science approved all the experimental procedures used in this study. After the training was completed, we implanted the observer bat with a microdrive (weight 2.1 g), loaded with four tetrodes, where each tetrode was constructed from four strands of insulated wire (17.8-µm diameter platinum–iridium wire), as described previously[25,35–38]. Tetrodes were gold-plated to reduce wire impedance to a range between 0.3 MΩ and 0.7 MΩ (at 1 kHz). We implanted the microdrive above the right dorsal hippocampus (3.1–3.5 mm lateral to the midline and 5.8–6.3 mm anterior to the transverse sinus that runs between the posterior part of the cortex and the cerebellum). Surgical procedures were similar to those described previously[25,35–39]. We used an injectable mixture of anesthetics composed of medetomidine 0.25 mg kg^{-1}, midazolam 2.5 mg kg^{-1} and fentanyl 0.025 mg kg^{-1} and subsequently added additional injections as needed, based on the bat's monitored vital signs. After surgery, over the course of the next 1–2 weeks, we lowered the tetrodes slowly toward the dorsal CA1 pyramidal cell layer while provisionally assessing the positions of tetrodes in the layer by the presence of high-frequency field oscillations ('ripples') and associated neuronal firing. Tetrodes advancement was done under visual inspection of electrophysiological signal in real time using Neuralynx Digital Lynx SX and Neuralynx Cheetah (version 6.3.0). Later, we also verified the tetrodes' positions histologically: the histology confirmed that all the tetrode tracks were localized in dorsal CA1 (see example in Extended Data Fig. 1e). For each bat, we left one tetrode as a reference in an electrically quiet zone. The remaining three tetrodes served as recording probes. During recordings, we attached a 16-channel wireless neural recording device ('neural logger', Deuteron Technologies) to an Omnetics connector on the microdrive. Signals from all 16 channels of the four tetrodes were amplified (×200) and band-pass filtered (1–7,000 Hz) and were then sampled continuously at 29.3 kHz per channel and stored onboard the neural logger. During subsequent processing, we further filtered the neural recording between 600 Hz and 6,000 Hz for spikes and then extracted 1-ms spike waveforms using a voltage threshold.

Spike sorting

All spike sorting procedures were identical to those described previously[22,25,35]. In brief, we sorted the spike waveforms based on their relative energies and amplitudes on different channels of each tetrode

(using the SpikeSort3D software from Neuralynx, version 2.5.2.0). Data from all sessions—the behavioral sessions and the sleep sessions that flanked the behavior—were spike sorted together. We manually selected well-isolated clusters of spikes and verified a refractory period (<2 ms) in the interspike interval histogram. We included only neurons that (1) were stably isolated throughout all the relevant sessions; (2) fired ≥40 spikes on at least one of the balls during the rest periods of the bat; and (3) had an average firing rate <10 Hz across the entire experiment (to exclude interneurons). Overall, 391 well-isolated, stable, active cells were recorded from dorsal hippocampal area CA1 of four observer bats.

Video tracking

The locations of the two bats (observer and demonstrator) were tracked simultaneously using two color cameras located at two of the upper corners of the room. The cameras were connected to a video tracker system (Neuralynx Cheetah VTS), which tracked the location of omnidirectional LEDs mounted on the bat's head. The video tracker operated at a 25-Hz rate and tracked the two bats separately by the colors of the LEDs: red LED on the observer bat and blue LED on the demonstrator bat. The video tracking data were synchronized with the neural data by recording a pseudo-random sequence of TTL pulses on both systems; this yielded a synchronization accuracy of <1 ms.

Data analysis

All the behavioral and neural data in this study were analyzed using custom code written in MATLAB.

Estimating the locations of the bats

We reconstructed the three-dimensional (3D) locations of the bats using the direct linear transform algorithm, applied to data from two cameras and two video trackers (Neuralynx Cheetah VTS)[25,36]. We identified individual flights by local peaks in the flight velocity that had maximal velocity >1.2 m s^{-1}. We defined landing and takeoff events by the local minima in the flight velocity at the beginning and end of each flight. We then correlated each flight with the average flight velocity profile. Flights with Pearson correlation of $r > 0.8$ were treated as valid, directed flights and were included in the analysis[25]; in particular, the takeoff moments and landing moments of these valid flights were used to delimit valid trials of the bats on the landing balls, which we then analyzed here. To improve the accuracy in estimating flight velocity, we smoothed the bat's location using a smoothing spline (csaps.m in MATLAB), based on which the instantaneous velocity was computed. The detection of landing moments and takeoff moments was performed identically for the observer bat and for the other bat (demonstrator). In this study, we aligned all the time plots to the landing moment of the bat (either self or other), except in Extended Data Fig. 2b where we aligned to the takeoff moment.

Definition of time cells

Time cells for self and for other were defined in the same manner. For analyzing time cells, we included only epochs when both bats were hanging motionlessly from the landing balls (Fig. 1c and Extended Data Fig. 1a–c). In our analysis, we used both correct (rewarded) trials and incorrect (non-rewarded) trials. To detect time cells, we first calculated the firing rate of each cell in each trial, aligned to the bat's moment of landing, and up to the moment of takeoff (with landing and takeoff as defined above in the section 'Estimating the locations of the bats'). The bats took off voluntarily, so the stationary delay times on the balls were highly variable in duration (Figs. 1d and 5d). We used time bins of 100 ms and smoothed the single-trial firing rates using a fixed Gaussian kernel ($\sigma = 2.5$ bins; we used temporally symmetric filtering with no time shift, using MATLAB's filtfilt.m function; to avoid edge effects during filtering, we computed the single-trial firing rate using long time margins before landing and after takeoff and then filtered it and then cut the margins after filtering). We then used the time course of the firing rate in each trial to construct the average time course of the firing rate of the cell, averaged across trials—that is, a 'post-stimulus time histogram' (PSTH); we termed this PSTH the 'temporal tuning curve' (see examples in Fig. 1e, bottom; Extended Data Fig. 2a, bottom row; Extended Data Fig. 3; Extended Data Fig. 4a, middle row; and Extended Data Fig. 9c). The temporal tuning curve was calculated independently for each of the three different locations in the room: landing balls A and B and the start ball. Note that, because the trial durations varied (Fig. 1d), the number of trials contributing to each time bin in the PSTH decreased monotonically over time; we calculated the temporal tuning curve using only time bins with at least ten trials. Significant time cells (either for self or for the other bat) were required to fulfil the following criteria. (1) Significance: The neuron had a significant firing rate in at least three consecutive time bins of 100 ms—that is, significant time field ≥300 ms (we note that 95.3% of the time fields were, in fact, significant for ≥1 second). To this end, we constructed a shuffle distribution for each bin. We shifted the instantaneous firing rate of each trial by a shift value that varied from zero to the trial duration, drawn from a uniform distribution; each trial was shifted rigidly and circularly by a different random shift value; we repeated this calculation 10,000 times, with shifts performed independently for each trial, to obtain the shuffle distribution for each time bin. We then compared the empirical average firing rate in each bin to its shuffle distribution. Time bins in which the temporal tuning curve was higher than the 99th percentile of the shuffle distribution were considered as significant time bins ($P < 0.01$; Bonferroni-corrected for multiple comparisons by the number of bins in the temporal tuning curve / 10 (where ten bins—that is, 1 second—is roughly the smallest field width in the data); significant time bins are shown as green rectangles in Fig. 1e, Extended Data Fig. 2a (bottom row), Extended Data Fig. 3 and Extended Data Fig. 4a,c (middle and bottom rows)). (2) Reliability: The time field of the cell was significant in at least 40% of the trials (to this end, we defined significant time bins for each trial as time bins that showed instantaneous firing rate ≥99th percentile of the shuffle distribution at the same time bin, Bonferroni-corrected as in (1)). Note that the mean number of trials per session for each landing ball was 44 trials. We also note that the temporal tuning was stable across trials (self: Fig. 1i; other: Fig. 5h). (3) The peak firing rate of the temporal tuning curve was ≥1 Hz. (4) The peak of the temporal tuning curve occurred after the moment of landing and before the last time bin of the temporal tuning curve. Thus, we defined a time cell—for both self and other—as a neuron that exhibited a statistically significant, large and stable transient firing at a particular moment of time after the bat's landing.

To identify time cells for self (observer bat), we used spikes recorded from neurons in the observer's hippocampal area CA1, aligned to the observer's landing moment (Extended Data Fig. 1b, top). To identify time cells for the other bat (demonstrator bat), we used spikes recorded from neurons in the observer's hippocampal area CA1, aligned to the demonstrator's landing moment (Extended Data Fig. 1b, bottom). As detailed above, we used the same criteria to define significant time cells for self and time cells for the other bat. We could not analyze time cells for the object because the object did not stay enough time on the balls.

The 'preferred time' of the time field was defined as the time of the field's peak firing rate. The 'field width' was defined as the width at half height of the time field. These are shown in red in Fig. 1e (bottom), Extended Data Fig. 2a (bottom row) and Extended Data Fig. 3. The preferred time is marked by the thin vertical red line, and the field width is marked by the thick red curve.

Controlling for observer bat movements

To control for effects of movements, we measured the head movements of the observer bat using a nine-axis motion sensor that was part of the neural logger on the observer's head; the motion sensor data were synchronized to the neural data with a microsecond-level precision.

This motion sensor included a three-axis accelerometer, which allowed measuring the observer's head movements at a 114.5-Hz sampling rate. The accelerometer signal was recorded on only a subset of the days (on 70.4% of experimental days in which significant time cells for self or other were identified). We note that the accelerometer on the bat's head measures very effectively not just head movements but also body movements, as the bats were hanging upside down, akin to a pendulum.

For computing the trial-to-trial correlations between the accelerometer signal and the firing time or firing rate (Fig. 2c or Extended Data Fig. 4b,d) and for computing the correlations between the accelerometer signal on different trials (Extended Data Fig. 4e,f), we downsampled the accelerometer signal to 10.4 Hz and then smoothed it with a Gaussian kernel ($\sigma = 1.5$ samples).

We performed several control analyses, which revealed the following. (1) Overall, the acceleration signal during the firing of time cells was flat (Extended Data Fig. 4a, bottom row, and Extended Data Fig. 4e), indicating that the bats were largely motionless when the time tuning was measured—that is, when the bats were hanging from the landing balls. (2) There was very low similarity between the acceleration profiles of pairs of trials recorded within the same session, indicating that the bats did not perform stereotypical movements across trials (Extended Data Fig. 4e,f; mean Pearson correlation: $r = 0.052$). (3) Only a few time cells showed any significant correlation between the trial-to-trial variation in firing rate and the trial-to-trial variation in the acceleration signal (Extended Data Fig. 4a–d). (4) There was no significant trial-to-trial correlation between the timing of peak acceleration and the timing of peak neuronal activity (Fig. 2c). (5) The spike-triggered accelerometer signal was flat (Fig. 2d), suggesting that these CA1 neurons do not carry a motor or premotor signal. (6) The firing of time cells is unlikely to reflect preparatory activity before takeoff, because these neurons fired reliably at specific times after landing (Fig. 1f,i), despite the large variability in takeoff times (Fig. 1d), and their firing was also not locked to takeoff (Extended Data Fig. 2b,c). (7) The firing of time cells is unlikely to be related to periodic behaviors, such as breathing or ear movements (Extended Data Fig. 4j), because time cells discharged only once per trial and did not fire periodically. Taken together, these results suggest that time cells encode the elapsed time from the moment the bat has landed, unrelated to movement.

Decoding analysis

We used a Bayesian maximum likelihood decoder[40] to decode time for the observer bat (Extended Data Fig. 5e,f). In Extended Data Fig. 5e, we decoded the elapsed time separately in each location in the room (balls A and B and start), independently for each time bin, from $t = 0$ to $t = 8$ seconds, using 200-ms time bins. For each time bin, we constructed the response vector r from the instantaneous spike counts of the ensemble of time cells that were tuned at that location in the room. The ensemble probability $Pr(r_i|t_j)$ was computed under the assumption of Poisson firing (which is a standard assumption in Bayesian decoding[40,41]) and was estimated using the tuning curve for each time cell, independently for each trial, via a leave-one-trial-out procedure (whereby, when we decoded trial k for a particular neuron, the temporal tuning curve was computed using all the trials for that neuron, except trial k). The decoded time was defined as the time that maximizes the log-likelihood function:

$$f(t_j) = \sum_{i=1}^{N} \log\left(Pr\left(r_i|t_j\right)\right)$$

where the index i runs over all the time cells tuned at that location, and j runs over all the time bins, from $t = 0$ to $t = 8$ seconds.

The decoding error was defined as the difference between the actual (real) time bin and the time bin that maximized the log-likelihood function. To estimate the temporal decoding error of elapsed time in Extended Data Fig. 5e (right), we computed the median decoding error over 1,000 repetitions in each time bin. In each repetition, the spike counts vector was composed of a different random selection of spike counts from an ensemble of time cells (one random trial per neuron). For decoding the elapsed time using all the time cells in Extended Data Fig. 5e (right, red line), the spike counts vector was composed of all the time cells that were tuned in one of the locations in the room; the location (and, hence, the set of tuned cells) was chosen randomly for each iteration. For decoding the elapsed time using contextual time cells in Extended Data Fig. 5e, right (peach-colored line), the spike counts vector was composed of all the contextual time cells that were tuned in one of the locations in the room; the location (and, hence, the set of contextual time cells) was chosen randomly for each iteration. Likewise, we also decoded the elapsed time using pure time cells only (Extended Data Fig. 5e, right (blue-colored line)).

In Extended Data Fig. 5f, we decoded the elapsed time using pure time cells whose preferred time on balls A and B differed by $\Delta T \leq 1$ second. For each trial in one location, we trained the decoder on the responses in the other location ('cross-decoding').

The grayscale values in the confusion matrices in Extended Data Fig. 5e, left, and Extended Data Fig. 5f represent the decoded probability divided by the uniform chance probability.

Place cells and social place cells

The spatial firing rate maps for place cells and social place cells were computed as described previously[25]. In brief, the firing rate maps (for example, Extended Data Fig. 7b, left) were constructed for flight periods only, separately for the two flight directions—that is, one map for the flights from the start ball to landing balls A and B and a separate map for the flights back. To ensure that takeoff and landing data did not contaminate the flight epochs, we removed from analysis the parts of the flight trajectory that were in the vicinity of the landing balls (~20-cm radius around each landing ball). To compute two-dimensionl (2D) classical place cell firing rate maps for the self bat (observer), we used spikes recorded from neurons in the observer's hippocampal area CA1 and the corresponding flight trajectories of the observer. To compute 2D firing rate maps for the other, demonstrator bat (that is, to analyze social place cells), we used spikes from neurons recorded in hippocampal area CA1 of the observer bat and the corresponding flight trajectories of the demonstrator (other) bat. We used fixed-sized spatial bins (10×10 cm^2) and collapsed the time spent (occupancy) data and the spike counts onto the horizontal 2D plane (x–y). We smoothed both the spike count and time spent 2D maps with a fixed Gaussian kernel ($\sigma = 1.5$ bins) and then divided, bin by bin, the smoothed 2D spike count map by the smoothed 2D time spent map, to obtain a firing rate map. Spatial bins (2D pixels) in which the bat spent <100 ms during the session were excluded from analysis and from the 2D firing rate map and were colored white. Significant place cells and social place cells were then identified based on spatial information as compared to shuffled distributions, as described in detail in ref. 25 (see example place cells in Extended Data Fig. 7b, left).

Detection of SWRs and removal of trials with ripples

To detect SWR events, the local field potential (LFP) signal was filtered between 100 Hz and 200 Hz, and the instantaneous power of the filtered signal was computed using the Hilbert transform. SWR events were defined by using two criteria. (1) We extracted events in which the power of the band-pass-filtered LFP (100–200 Hz) exceeded a threshold of 3 s.d. above the mean power. (2) We used a 'ripple/high gamma ratio'—the ratio between the peak power of the LFP signal between 100 Hz and 200 Hz (ripple range) and the peak power of the LFP between 60 Hz and 100 Hz (high gamma range)—and required a ratio of >1.5 to discern clear spectral peaks in the ripple range. Only candidate SWR events that met both criteria were selected for further analysis. To assess the possible contribution of SWR events to the firing of time cells, we recalculated the temporal tuning curves by using

only ripple-free trials and compared them to temporal tuning curves calculated using all trials (Extended Data Fig. 2g,h).

Statistics

No statistical methods were used to pre-determine sample sizes, but our sample sizes (both the number of animals and the number of neurons) are similar to those reported in previous publications, in both rodents and bats[6,7,42–44]. Data distribution was assumed to be normal, but this was not formally tested. In a few cases where the data did not seem normally distributed, we used non-parametric tests (see below).

Significant time fields were detected using a shuffling method (99th percentile, Bonferroni-corrected), as detailed above. We used the Wilcoxon rank-sum test everywhere for comparing the medians of distributions. We used the Kolmogorov–Smirnov test everywhere for comparing the shapes of distributions. We used the Pearson correlation coefficient for estimating correlations, except a few cases where the data did not seem normally distributed, in which case we reported both the Pearson correlation and the non-parametric Spearman correlation. We used a non-parametric *F*-test (Ansari–Bradley test) to test for equal variances in the distributions of time differences between different landing balls ($\Delta T_{\text{pref-time}}$) in Figs. 4c,d and Fig. 5l and Extended Data Fig. 8g–i. We used the Hartigan's dip test for unimodality[45] to test whether the distribution in Fig. 4e is unimodal. In Extended Data Fig. 6f, we used the log-odds ratio test for testing the difference in the percentage of time cells between sessions 1 and 2. All the statistical tests were two-sided, unless otherwise indicated.

Data collection and analysis were not performed blinded to the conditions of the experiments. The study did not involve experimental groups, and, therefore, no randomization and no blinding were required. No animals and no data points were excluded from the analyses in this study, except as described above in the section 'Definition of time cells', where we defined the inclusion criteria for time cells.

Reporting summary

Further information on research design is available in the Nature Portfolio Reporting Summary linked to this article.

Data availability

All the behavioral and neural data in this study are available from the authors upon reasonable request and are also accessible online at Zenodo[46].

Code availability

All the behavioral and neural data in this study were analyzed using custom code in MATLAB (version 2021b). The code that supports the conclusions of this study is available from the authors upon reasonable request and is also accessible online at Zenodo[46].

References

35. Yartsev, M. M., Witter, M. P. & Ulanovsky, N. Grid cells without theta oscillations in the entorhinal cortex of bats. *Nature* **479**, 103–107 (2011).
36. Yartsev, M. M. & Ulanovsky, N. Representation of three-dimensional space in the hippocampus of flying bats. *Science* **340**, 367–372 (2013).
37. Finkelstein, A. et al. Three-dimensional head-direction coding in the bat brain. *Nature* **517**, 159–164 (2015).
38. Sarel, A., Finkelstein, A., Las, L. & Ulanovsky, N. Vectorial representation of spatial goals in the hippocampus of bats. *Science* **355**, 176–180 (2017).
39. Tuval, A., Las, L. & Shilo-Benjamini, Y. Evaluation of injectable anaesthesia with five medetomidine–midazolam based combinations in Egyptian fruit bats (*Rousettus aegyptiacus*). *Lab. Anim.* **52**, 515–525 (2018).
40. Dayan, P. & Abbott, L. F. *Theoretical Neuroscience: Computational and Mathematical Modeling of Neural Systems* (MIT Press, 2001).
41. Davidson, T. J., Kloosterman, F. & Wilson, M. A. Hippocampal replay of extended experience. *Neuron* **63**, 497–507 (2009).
42. Ginosar, G. et al. Locally ordered representation of 3D space in the entorhinal cortex. *Nature* **596**, 404–409 (2021).
43. Dotson, N. M. & Yartsev, M. M. Nonlocal spatiotemporal representation in the hippocampus of freely flying bats. *Science* **373**, 242–247 (2021).
44. Sarel, A. et al. Natural switches in behaviour rapidly modulate hippocampal coding. *Nature* **609**, 119–127 (2022).
45. Hartigan, J. A. & Hartigan, P. M. The dip test of unimodality. *Ann. Stat.* **13**, 70–84 (1985).
46. Omer, D. B., Las, L. & Ulanovsky, N. Data for 'Contextual and pure time coding for self and other in the hippocampus' https://doi.org/10.5281/zenodo.7213099 (2022).

Acknowledgements

We thank Y. Dudai, Y. Ziv, S. Ray, S. R. Maimon, G. Ginosar, A. Sarel, T. Eliav, A. Rubin, A. Ravia, S. Palgi and J. Aljadeff for discussions and comments on the manuscript; S. Kaufman, O. Gobi, S. Futerman and E. Solomon for bat training; A. Tuval for veterinary support; C. Ra'anan and R. Eilam for histology; G. Ankaoua and B. Pasmantirer for mechanical designs; and G. Brodsky for graphics. N.U. holds the Barbara and Morris Levinson Professorial Chair in Brain Research. This study was supported by research grants from the European Research Council (ERC-CoG – NATURAL_BAT_NAV) to N.U. and the Israel Science Foundation (ISF 1920/18) to N.U. and L.L. and by the André Deloro Prize for Scientific Research and the Kimmel Award for Innovative Investigation to N.U.

Author contributions

D.B.O., L.L. and N.U. designed the project. D.B.O. performed the experiments and analyzed the data, with major input from N.U. and L.L. D.B.O. and N.U. wrote the manuscript, with major input from L.L. N.U supervised the project.

Competing interests

The authors declare no competing interests.

Additional information

Extended data is available for this paper at https://doi.org/10.1038/s41593-022-01226-y.

Supplementary information The online version contains supplementary material available at https://doi.org/10.1038/s41593-022-01226-y.

Correspondence and requests for materials should be addressed to David B. Omer or Nachum Ulanovsky.

Peer review information *Nature Neuroscience* thanks James Heys and the other, anonymous, reviewer(s) for their contribution to the peer review of this work.

https://doi.org/10.1038/s41593-022-01226-y

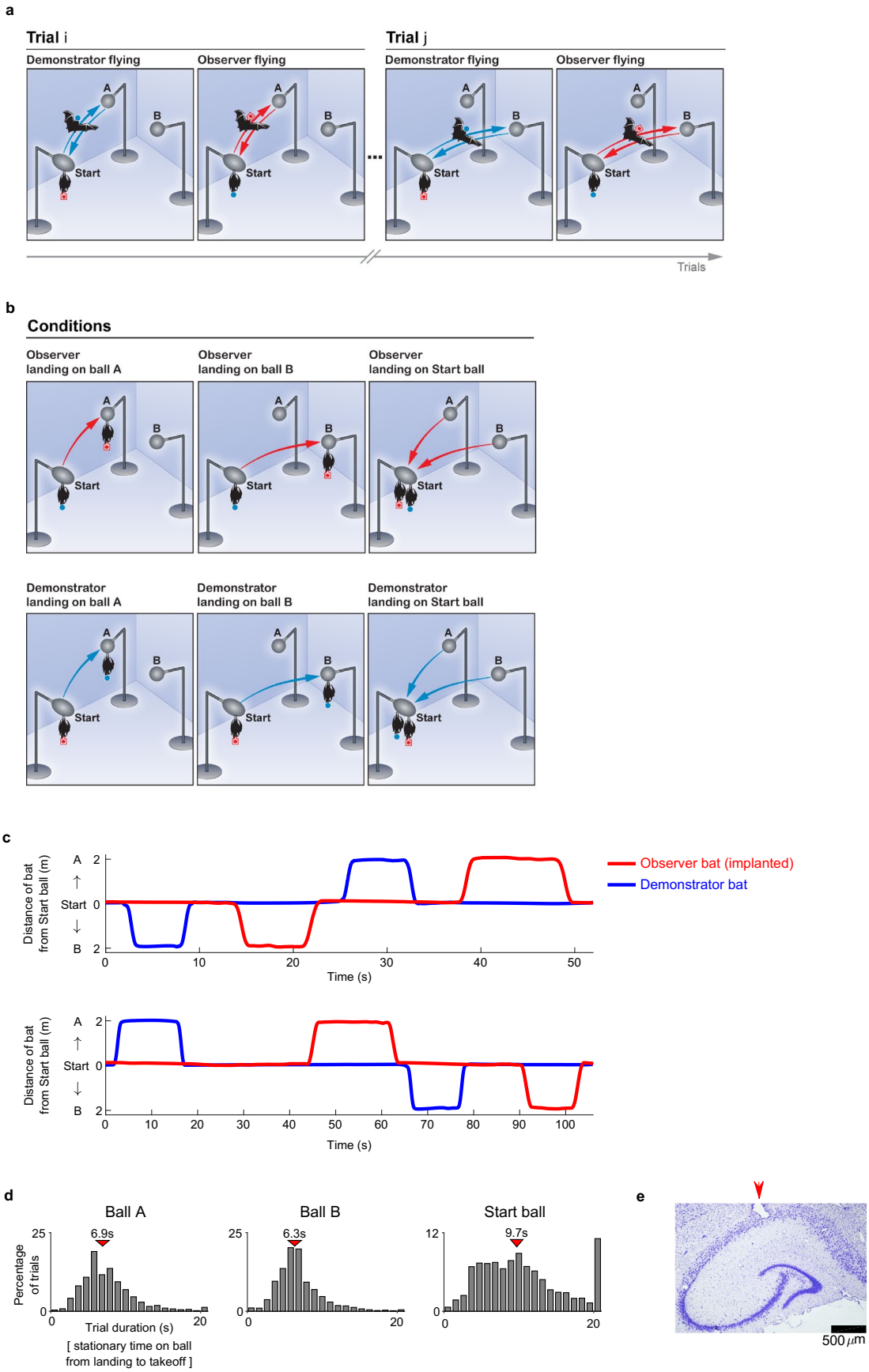

Extended Data Fig. 1 | See next page for caption.

https://doi.org/10.1038/s41593-022-01226-y

Extended Data Fig. 1 | Behavioral setup, conditions, and behavior. (a) Behavioral setup. Bats flew inside a flight-room (2.35 × 2.69 × 2.56 m, seen here from top side view). The demonstrator bat (blue) was trained to fly from the Start ball, roughly randomly to either landing-ball A or B, and back. The observer bat was trained to watch, remember and imitate the ball-choices of the demonstrator bat. Different trials are shown, one to ball A (trial *i*) and one to ball B (trial *j*). Balls and bats are not drawn to scale, for display purposes. **(b)** The six different conditions which were used to identify and analyze time-cells. Top row: the 3 conditions which were used to analyze self-time-cells. In each of these 3 conditions, the firing activity of cells recorded in dorsal CA1 of the observer bat was aligned to the landing moment of the observer bat on one of the landing-balls (columns). Bottom row: the 3 conditions which were used to analyze time-cells for the other bat. In each condition, the firing activity of cells recorded in the observer's dorsal CA1 was aligned to the landing moment of the other bat, the demonstrator. To enhance the clarity of reading the main text, we re-plotted the top row of panel b also in main Fig. 1b, and re-plotted the bottom row of panel b also in main Fig. 5a. **(c)** Two examples of bat behavior from the experiment. For each example: *x*-axis is the elapsed time in seconds; *y*-axis shows the distance in meters of each bat (demonstrator in blue, observer in red) from the Start ball. For clarity, the distances during roundtrips to balls A or B were plotted with opposite signs (A – positive distances, B – negative distances). In the top example, the two bats flew alternatingly from the Start ball to ball B and back and then to ball A and back; in the bottom example, the opposite order occurred: they first flew to ball A and then to ball B. **(d)** Distribution of trial durations in each of the three locations in the room (A, B and Start; shown is the time spent by the observer-bat on each of the landing-balls, from the moment of landing to takeoff); the rightmost bin corresponds to trial-durations ≥ 20 s. The median trial-duration in each location was marked by a red arrowhead. **(e)** Coronal Nissl-stained section through dorsal hippocampus of one observer bat. Arrowhead, electrolytic lesion at the end of a tetrode-track, located in dorsal CA1.

https://doi.org/10.1038/s41593-022-01226-y

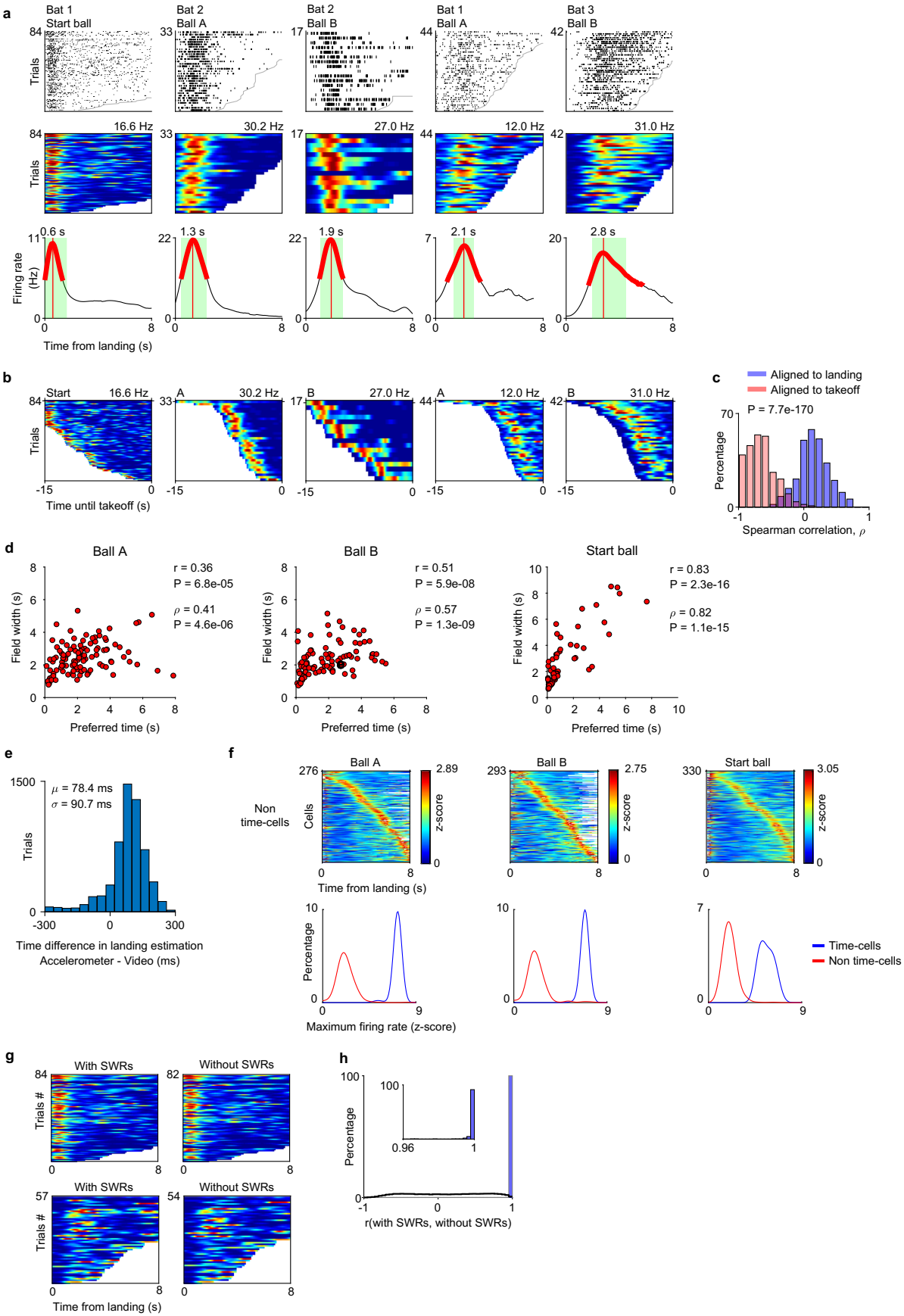

Extended Data Fig. 2 | See next page for caption.

https://doi.org/10.1038/s41593-022-01226-y

Extended Data Fig. 2 | The duration of time-fields increased with the neuron's preferred-time; analysis of non time-cells; and control for sharp-wave ripples. (a-d) The temporal resolution of time-cells deteriorated with the passage of time. **(a)** Examples: Spike rasters (top), color-coded rasters (middle), and temporal tuning-curves (bottom) for a subset of the time-cells from Fig. 1f. Each column represents one time-cell. Top row – Spike rasters: *x*-axis, elapsed time from the moment the bat has landed (time 0); *y*-axis, repeated landings (trials). Each raster corresponds to a single location in the room (indicated above the raster), and each line in the raster shows the spiking activity in a single trial; each tick represents one spike. The trials in each raster were sorted according to trial-duration; the thin gray line denotes the trial-end (shown are only spikes contained within the trial). Middle row – Color-coded rasters: arranged as the spike-rasters above, but showing the instantaneous firing-rate instead of raw spikes (100 ms time-bins). Plotted as in Fig. 1e; color-scale ranges from zero (blue) to the maximal firing-rate in each panel (red; maximal rate indicated). Bottom row – Temporal tuning-curve for each cell (black trace), which is the averaged firing-rate of the neuron (average of the color-coded raster above). The preferred-time is indicated above the peak-firing of each cell (marked also by a vertical red line). Green shading represents statistically-significant time bins (Methods). Red curve, width-at-half-height of the time-field. Note how the width of the time-field (duration of the red curve) increases with a neuron's preferred-time. **(b-c)** Plots showing that time-cells are aligned to landing, and not to takeoff. **(b)** Examples: color-coded rasters for the same cells as in panel a, aligned here to the bat's takeoff. *x*-axis, elapsed time until the moment the bat took off (time 0); *y*-axis, repeated landings (trials). Each line in the raster represents the firing-rate for the cell in a single trial. The trials in each raster were sorted according to trial-duration (same sorting as in panel a). Color-scale ranges from zero (blue) to the maximal firing-rate in each panel (red; maximal rate indicated). Note that the peak firing across trials is diagonally tilted, and is aligned to landing and not to takeoff. **(c)** Distributions of Spearman correlations between the time of peak-firing in each trial and the trial-number (ordered by trial-duration). Cells whose firing is truly aligned to landing are expected to show zero correlation when the rasters are aligned to landing (as seen in the example rasters in panel a) and a negative correlation when the rasters are aligned to takeoff (as seen in the negative correlations in the examples in panel b). The distributions in the current panel were plotted for all the significant time-cell rasters ($n = 274$ cells × positions), separately when the rasters are aligned to landing (blue) or aligned to takeoff (pink). Note that, as expected, the distribution for rasters that we aligned to takeoff was significantly shifted towards −1, as compared to the distribution for rasters aligned to landing (two-sided *t*-test: $P = 7.7 \times 10^{-170}$) – indicating that time-cell rasters show vertical bands when aligned to landing (as in panel a), and are tilted when aligned to takeoff (as in panel b); this means that the time-cells are tuned to the elapsed time from landing, rather than to time-until-takeoff (the small rightward shift in the blue histogram occurs because of late noisy firing in longer trials, as seen for example in panel a, fourth cell, which biases the correlations positively). Furthermore, since the time-cells in this analysis were defined based on the alignment of their firing to landing, we performed an additional analysis without such definition – to test whether takeoff (departure) can also trigger time-sequences, perhaps in a different set of neurons. To this end, we aligned the activity of all the neurons to the takeoff instead of landing, and sought to identify significant responses with this new alignment. We used in this analysis the exact same time-binning and same criteria to detect pure time-cells, contextual time-cells, and social time-cells, as we used for 'landing-triggered' time-cells throughout the paper – but now aligned on takeoff. This analysis yielded a substantially lower number of significant time-cells from each class: we found only 13 significant pure time-cells when aligned to takeoff versus 44 pure time-cells when aligned to landing; only 65 contextual time-cells when aligned to takeoff versus 125 contextual time-cells when aligned to landing; and only 28 social time-cells when aligned to takeoff versus 56 social time-cells when aligned to landing (all numbers are cells, not cells × positions). This much-lower percentage of significant cells when aligning to takeoff versus landing, strongly suggests that the relevant trigger for time-cells is landing and *not* takeoff. **(d)** Scatter plots of the time-field duration (field width at half-height) versus the preferred time, for all the significant time-fields (dots), in each of the three locations in the room: ball A (left; $n = 116$ significant time-fields), ball B (middle; $n = 98$), and Start ball (right; $n = 61$). All three scatter-plots showed significant positive correlations: ball A: Spearman $\rho = 0.41$, $P = 4.6 \times 10^{-6}$; ball B: $\rho = 0.57$, $P = 1.3 \times 10^{-9}$; Start ball: $\rho = 0.82$, $P = 1.1 \times 10^{-15}$ (two-sided tests) (the significant positive correlations persisted also after eliminating from the correlations those time-cells with preferred time < 0.5-s: ball A: $\rho = 0.24$, $P = 0.01$; ball B: $\rho = 0.46$, $P = 2.4 \times 10^{-5}$; Start ball: $\rho = 0.77$, $P = 4.6 \times 10^{-9}$). This demonstrates that in each of the 3 locations in the room (A, B, Start), the time-resolution of time-fields deteriorated with the passage of time – as reported also for time-cells in rats[7,8,10,17]. **(e)** Distribution of the time differences ΔT between the estimated time of landing from the video data and the estimated time of landing from the accelerometer signal (mean and standard deviation of ΔT: μ = 78.4 ms; σ = 90.7 ms; $n = 5695$ trials; the video-based landing time [our main estimate of landing-time in this study] was explained in the Methods – and the accelerometer-based landing time was estimated as the peak in the accelerometer signal, which exceeded $1.5 \times g$ (1.5 times the Earth's gravitational acceleration), and occurred within a time window of ± 300 ms around the video-based landing-time). Note that the standard deviation of this distribution was less than the time-bin resolution (100-ms bins) that we used for computing the temporal tuning-curves of the time-cells – indicating a very precise estimation of the landing-time. **(f)** Non time-cells. Top row: Temporal firing pattern of all the non-time-cells, plotted as in Fig. 1g: the cells are plotted separately for each of the landing-balls, and are ordered by the time of their peak firing-rate. Bottom row: the distributions of peak *z*-scores for time-cells (blue curves) and non time-cells (red curves). The firing sequences of non-time cells were clearly very different from the firing sequences of the significant time-cells shown in Fig. 1g: The *z*-scores were dramatically lower for non time-cells as compared to time-cells. In addition, the sequences of non-time cell tended to fall close to the diagonal in the top row. Both of these differences indicate that non time-cells do *not* exhibit true temporal tuning. (**g**-**h**) Sharp-wave ripples (SWRs) do not generate the temporal responses of time-cells. (**g**) Examples of two time-cells (rows), showing high similarity when plotted with versus without trials that included SWRs (columns; compare left versus right; example cells are from bat 1 [top row] and bat 2 [bottom row]). **(h)** Distribution of Pearson correlation coefficients between the temporal tuning-curves of time-cells when computed using all trials versus when computed after removal of trials with SWRs. Blue histogram, correlations for the data for all time cells ($n = 274$ cells × positions; note that the rate of SWRs was very low and they occurred only on a small subset of the trials: on average 0.97% of the trials). Black line, distribution of correlations for cell-shuffling (correlation between the temporal tuning-curve computed over all trials for cell i and the temporal tuning-curve computed over trials without SWRs for cell j, for $i \neq j$). The real data correlations were significantly higher than the shuffles (two-sided *t*-test with unequal variances: $P < 10^{-300}$; $t = 485.2$; $df = 7.4 \times 10^4$). Inset: enlarged view of the blue histogram (zoom-in on the *x*-axis between 0.96 – 1). These high correlations indicate that the temporal tuning of time cells could not be explained by the occurrence of sharp-wave ripples.

https://doi.org/10.1038/s41593-022-01226-y

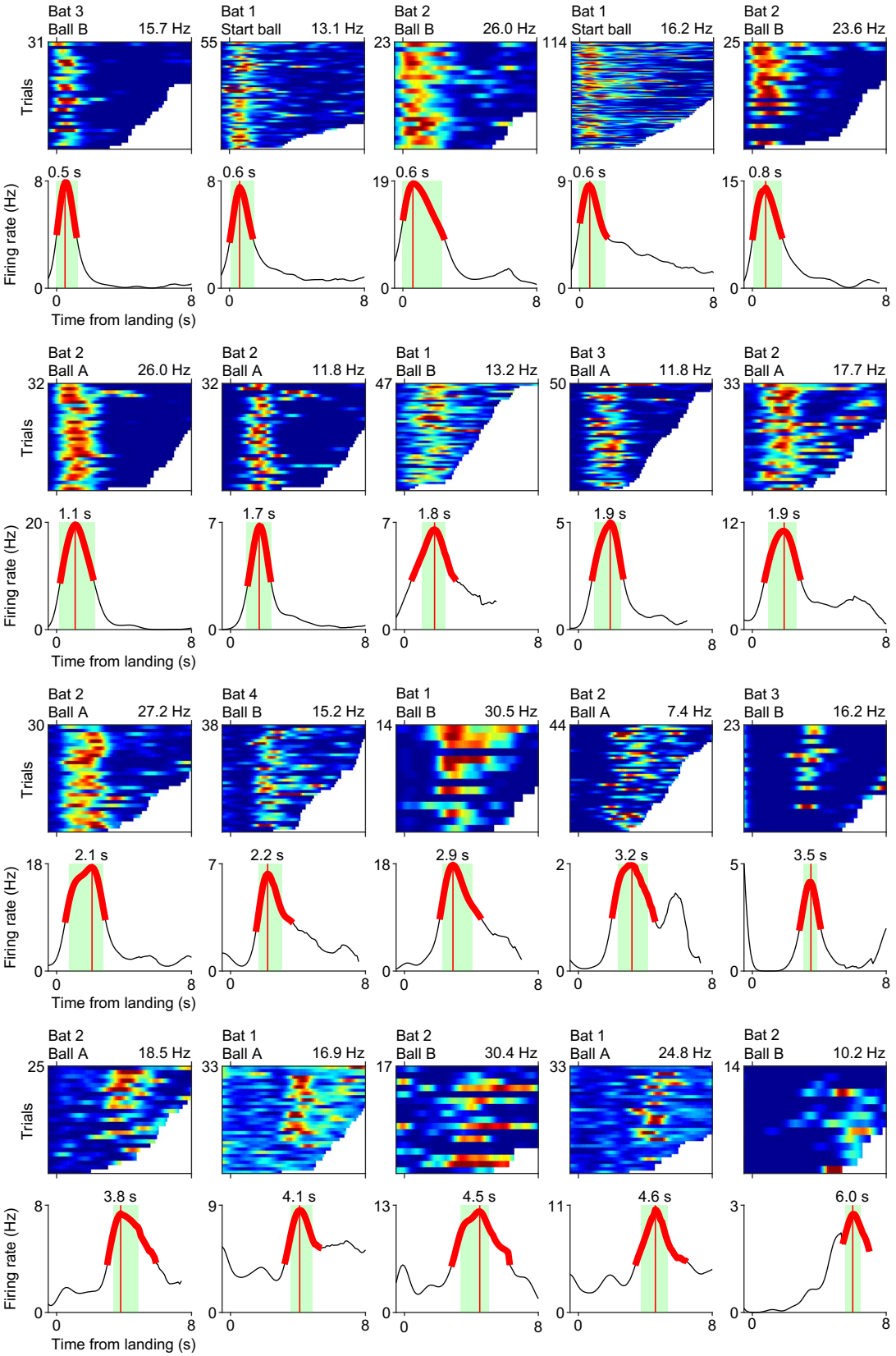

Extended Data Fig. 3 | Additional 20 examples of self time-cells. For each example cell, the top panel shows the color-coded raster plot: *x*-axis, elapsed time from the moment the bat has landed (time 0); *y*-axis, repeated landings (trials); plotted as in main Fig. 1e. The bottom panel shows the temporal tuning-curve (black trace), which is the averaged firing-rate of each cell (average of the color-coded raster above); the preferred-time is indicated above the peak-firing of each cell (marked also by a vertical red line); green shading represents statistically-significant time bins; red curve shows the width-at-half-height of the time-field. Cells were sorted by increased preferred times (from top-left to bottom-right panel).

https://doi.org/10.1038/s41593-022-01226-y

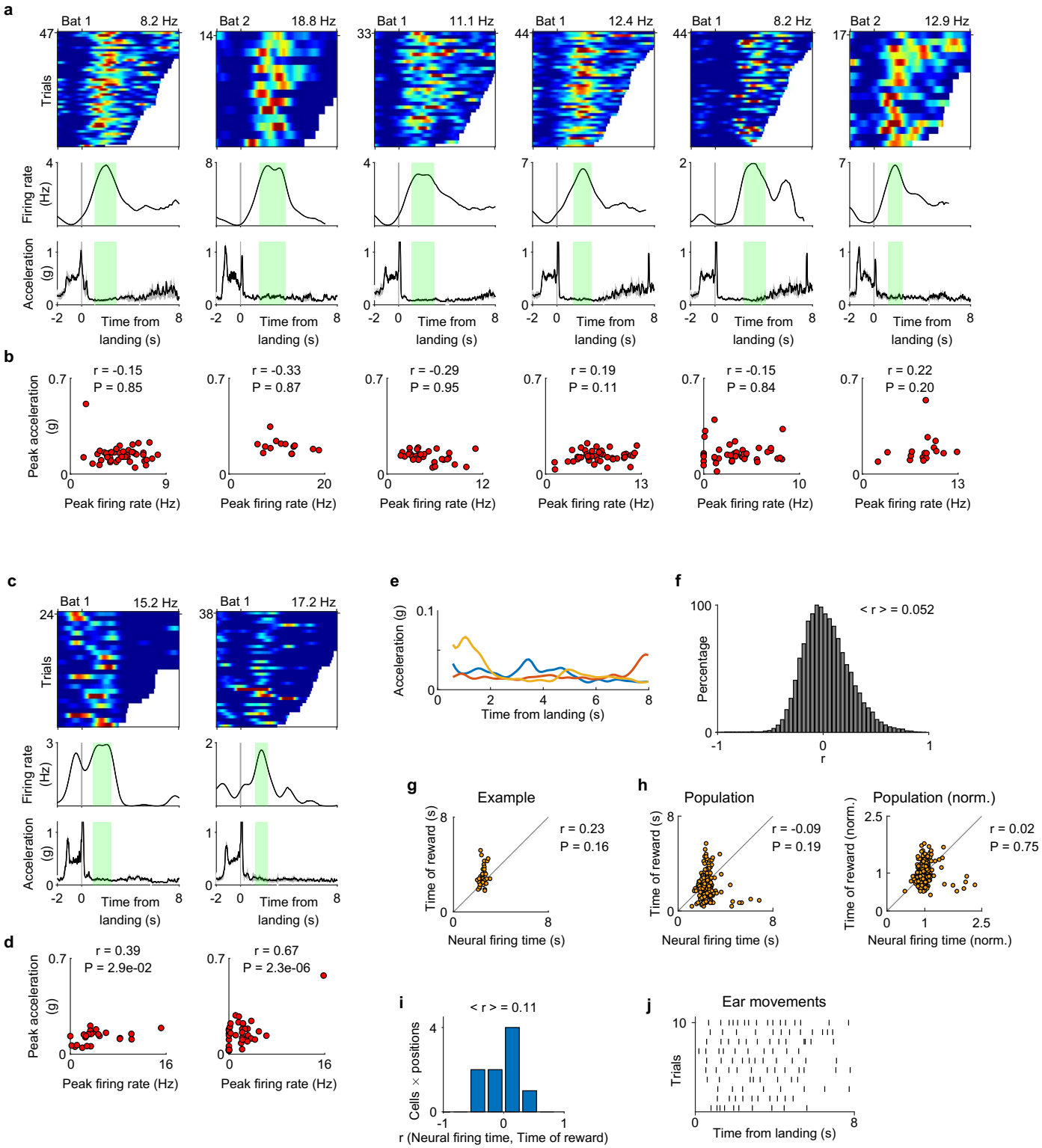

Extended Data Fig. 4 | See next page for caption.

https://doi.org/10.1038/s41593-022-01226-y

Extended Data Fig. 4 | Time-fields represent an internally-generated signal, not linked to movement. (a-d) Only 12.0% of the 133 time-cells [cells × positions] that were recorded together with an accelerometer signal (16/133 cells) showed significant correlation between the trial-to-trial variation in firing-rate and the trial-to-trial variation in the acceleration signal. **(a-b)** Six typical time-cells (columns) that showed no significant correlation between the trial-to-trial variation in firing-rate and the trial-to-trial variation in the acceleration signal. **(a)** Top: color-coded raster plot, aligned to the moment of landing ($t = 0$). Trials (y-axis) are sorted according to the trial duration. Plotted as in main Fig. 1f. Middle: temporal tuning-curves – the average firing-rate across all recorded trials, aligned to the moment of landing of the observer bat. Green shading represents statistically-significant time bins. Bottom: acceleration signal, averaged across trials (gray shading, mean ± SEM). The acceleration signal shown here included flight-data for $t < 0$, while for $t > 0$ we only included here data recorded when the bat was on the ball (before takeoff). Note the large acceleration signal prior to landing (prior to $t = 0$) in all cases, which is caused by the bat's flight – but then during the significant time bins (green shading) there was basically no acceleration signal. In other words, the bats hardly moved during the firing of the time-cells. All three panels for each cell (top, middle, bottom) are aligned to the landing-moment ($t = 0$) and to each other. **(b)** Six example scatter plots (for the 6 cells in panel a), showing that there is no significant correlation between the trial-to-trial variation in peak firing-rate and the trial-to-trial variation in the peak acceleration signal (both the peak firing-rate and the peak acceleration signal were measured inside the green rectangles in panel a; we used here a one-sided test for the Pearson correlation, and not two-sided test, because we assumed that only positive correlations are physiologically meaningful). These six examples represent the typical majority of time-cells that we recorded in experiments with accelerometer signal – which showed no trial-to-trial correlation between firing-rate and acceleration. This indicates that time-cells represent an internally-generated signal, unrelated to movement. **(c-d)** Examples of two rare neurons (columns) which represent the small minority of time-cells that showed a significant correlation between the trial-to-trial variation in firing-rate and the trial-to-trial variation in the acceleration signal. Plotted as in panels a and b. **(c)** Color-coded rasters, temporal tuning-curves, and acceleration signals – plotted as in panel a. **(d)** Scatters, plotted as in b. The example cell on the right showed the highest correlation value among all our neurons ($r = 0.67$); we note, however, that when removing the outlier point, the correlation became non-significant ($r = 0.23$, $P = 0.16$). **(e-f)** The bats did *not* perform on the balls stereotypical movements that were similar across trials – suggesting that stereotypical movements could not explain the firing of time-cells. **(e)** Examples: Three acceleration traces recorded on three different trials on the same day, all from the same ball (a significant time-cell was recorded on that day on the same ball). Note that in these three example traces: (i) the acceleration values were extremely low (<0.1 g, where g is the Earth's gravity), and (ii) the traces were not similar to each other – indicating that this bat did not exhibit stereotypical movements across trials. **(f)** Population: Distribution of Pearson correlations between the acceleration signals recorded on different trials of the same day, on the same ball (computed from 0.5-s until trial-end; $n = 39{,}323$ trial-pairs) – that is, correlations between acceleration-traces as plotted in panel e. The correlation values were pooled across landing balls A and B and across experimental days and bats – only for days and balls on which a significant time-cell was recorded. The correlation of the acceleration signal between the different trials was very low (mean $< r > = 0.052$) – indicating that there were no stereotypical movements across trials that could explain the firing of time-cells. **(g-i)** No relation between time of firing and time of reward. **(g)** A typical example neuron showing no significant correlation between the time of peak neuronal firing (x-axis) and the time of reward delivery after landing (y-axis; extracted from the raw videos), with dots showing individual trials (Pearson $r = 0.23$; two-sided t-test, $P = 0.16$; $n = 38$ trials). Note there was large variability in the time-of-reward (large spread along the y-axis), as compared to the small variability in the neuron's time of firing across the trials (small spread along the x-axis). **(h)** Left panel, scatter plot, showing a similar plot as in panel g (with dots showing individual trials), pooled across all the example cells shown in main Fig. 1. Right panel, same scatter as on the left, but here the x-axis data and y-axis data for each neuron were normalized by the mean for that neuron, in order to expose possible correlations which may be masked due to the high variability of preferred-times across different neurons. Both scatters show a lack of significant trial-to-trial correlation between the time of firing for each time-cell and the time of reward on the same trial. In addition, the timing of reward-delivery was highly variable, arguing against a role for reward in the temporal tuning of time-cells. **(i)** Histogram showing the distribution of Pearson correlation coefficients between the time of peak firing and the time of reward delivery – like the correlation for the cell shown in panel g – plotted here for all the example cells shown in Fig. 1 (in panels h and i, shown are $n = 9$ cells for which we also recorded raw video movies in addition to the video-tracking; this raw-video footage was used to measure the time of reward). Almost all these cells (except one) showed *non*-significant correlation ($P > 0.05$). **(j)** Raster of the times of ear-movements (x-axis) that were measured across 10 randomly-chosen landing trials (y-axis); the measurements were performed manually from high-speed camera recordings at 100 frames/second. This raster shows that, first, ear movements are generally repetitive – and hence cannot explain the firing of time-cells, which always fire only once per trial, rather than repetitively; and second, ear movements do not show stereotypical structure across trials (note the lack of vertical bands in this raster) – and therefore ear movements cannot underlie the temporally-reproducible, distinct firing of time-cells.

https://doi.org/10.1038/s41593-022-01226-y

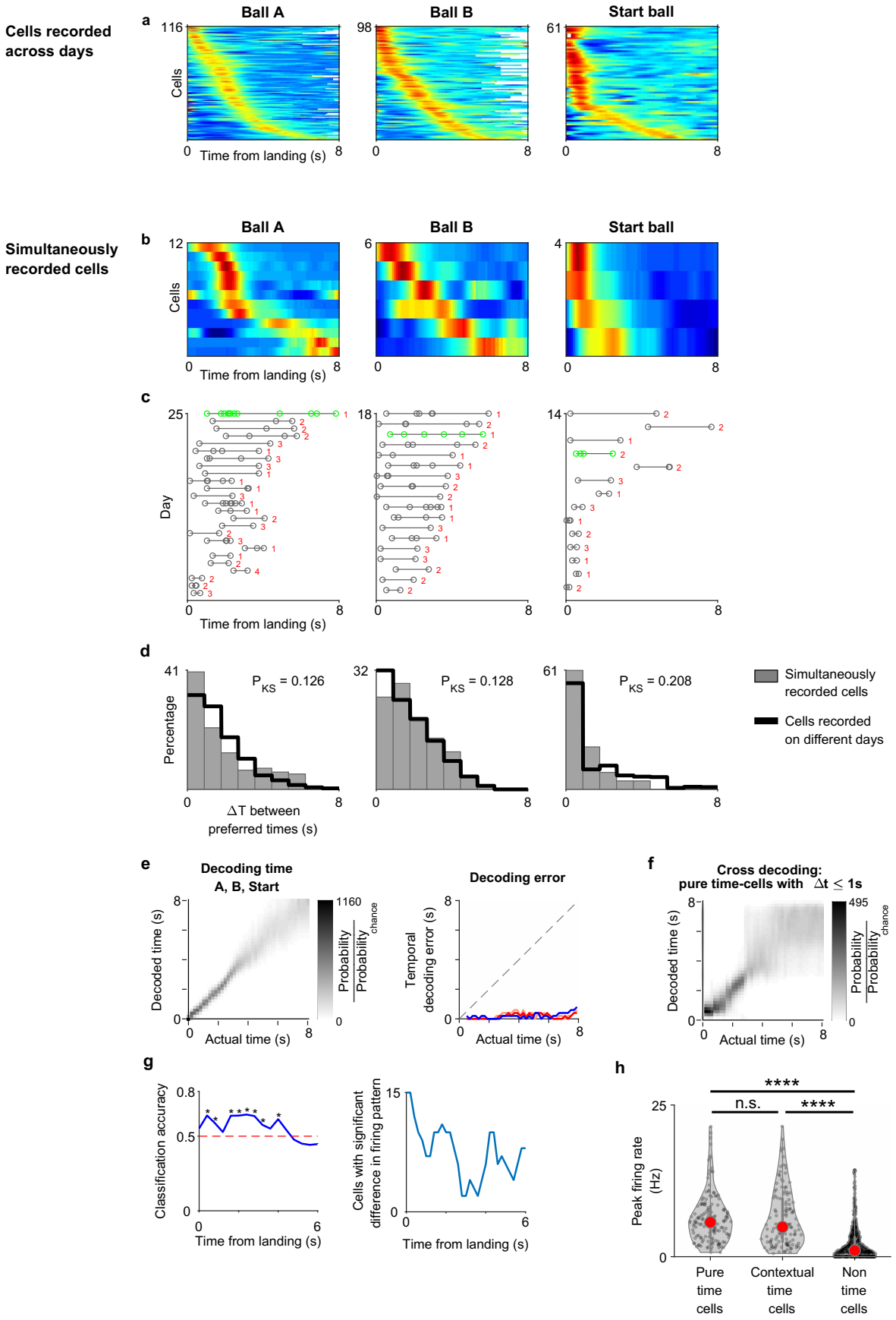

Extended Data Fig. 5 | See next page for caption.

https://doi.org/10.1038/s41593-022-01226-y

Extended Data Fig. 5 | Firing sequences in simultaneously recorded time-cells are similar to the population time-cell sequences pooled across all days; and decoding elapsed-time from time cells. (a) Temporal tuning curves for all the significant time-cells, pooled across all experimental days and bats (the 3 panels correspond to the 3 different locations in the room: balls A, B and Start). These plots are identical to those shown in main Fig. 1g, and were plotted here again to facilitate comparison with panel b. **(b-d)** Simultaneously-recorded time-cells. **(b)** Three examples of internally-generated temporal sequences, for ensembles of neurons that were recorded simultaneously: These examples depict similar sequences (with a similar time-span) to the population in panel a. These 3 ensembles were recorded on 3 different recording-days, in the 3 different locations in the room (balls A, B, Start). We could not obtain larger numbers of simultaneous neurons because of the limited number of tetrodes in this study ($n = 4$ tetrodes; we obtained up to 12 simultaneously recorded significant time-cells per day). **(c)** All the days × locations (for all bats) in which we had ≥ 2 simultaneously recorded time-cells ($n = 57$ days × locations). The 3 panels represent the 3 locations in the room. *x*-axis, preferred time for each neuron (circles); *y*-axis, experimental day; horizontal lines in each panel represent groups of simultaneously recorded time-cells. Experimental days are sorted according to the total span of preferred-times for the time-cells recorded on that day. Green: the 3 examples in panel b of internally-generated firing sequences. The red numbers on the right indicate the identity of the bat (no. 1–4) from which the cells were recorded. **(d)** Distributions of time-differences (ΔT) between the preferred-times for all the cell-pairs recorded simultaneously on the same day (gray bars; $n = 151$, 109 and 23 cell-pairs on landing balls A, B and Start respectively), and all the cell-pairs recorded on different days (black lines; $n = 12800$, 9288 and 3614 cell-pairs on landing balls A,B and Start respectively), plotted separately for the 3 locations in the room. The gray and black distributions were statistically indistinguishable (two-sided Kolmogorov-Smirnov tests: $P = 0.126$, $P = 0.128$ and $P = 0.208$, for balls A, B and Start, respectively). This demonstrates that the pooled sequences (main Fig. 1g) are reliably representing the within-day sequences – indicating that time-cells in the bat hippocampus form internally-generated firing sequences. **(e)** Bayesian maximum-likelihood decoding of elapsed time. Left panel: Confusion matrix showing the decoded time (*y*-axis) versus the actual elapsed time (*x*-axis), using all the time cells, in all three locations. The probabilities in each time-bin were divided by the uniform chance probability. Right panel: Temporal decoding error for each time bin (200-ms bins were used here), computed between 0–8 s, for three cell groups: red line, all the time-cells ($n = 274$ cells × positions); peach line, contextual time-cells only (cells that were time-tuned in only one location; $n = 123$ cells × positions); blue line, pure time-cells only (cells that were time-tuned on both A *and* B; $n = 88$ cells × positions). Note the temporal decoding error was < 0.6 s for all the time bins up to 8 s – indicating that these neurons carry robust information about elapsed time, up to 8 s after landing. **(f)** Cross-decoding of elapsed time: For each trial we trained a decoder on responses at the *other* location. Only pure time-cells with preferred-time difference of $\Delta T \leq 1$ s between locations were used to train the decoder. The confusion matrix shows the decoded time (*y*-axis) versus the actual elapsed time (*x*-axis); the decoded probabilities in each time-bin were divided by the uniform chance probability. **(g)** Bayesian maximum-likelihood decoding of the origin of flight history – namely, decoding from where did the bat fly to the Start ball – this decoding was performed based on the firing of time-cells when the bat was on the Start ball. Left panel: the identity of the previous landing ball (ball A or B) can be decoded (classified) above chance level during the first ~4 seconds after landing on the Start ball. To assess the statistical significance of decoding in each time bin, we compared the observed classification accuracy to a shuffle test where we randomly permuted the true identities of balls A and B from which the bat flew. We repeated the shuffling 1,000 times and calculated the classification accuracy for each of the 1,000 shuffle-repeats (permutations) in each time bin. Asterisks denote time bins in which the empirically-observed classification accuracy showed significance at 95% [two-sided] compared to the distribution of classification accuracy of the shuffle tests (the observed classification accuracy was higher than the accuracy of 997.5 of the shuffles – Bonferroni-corrected for multiple comparisons for the number of time bins; $P < 0.0025$). Right panel: the number of time-cells, in each time bin, which showed significant difference in their firing-rate between trials when the bat flew from ball A to the Start ball versus from ball B to the Start ball. These results support the notion that time-cells encode relevant behavioral information. **(h)** Violin plots showing the distributions of peak firing-rates for pure time-cells, contextual time-cells, and non-time cells ($n = 151$, 123, and 603 cells × positions, respectively). Dots, individual neurons (cells × positions); red circles, median for each cell group. Peak firing-rate plotted in this panel is the peak of the temporal response (temporal tuning-curve).

https://doi.org/10.1038/s41593-022-01226-y

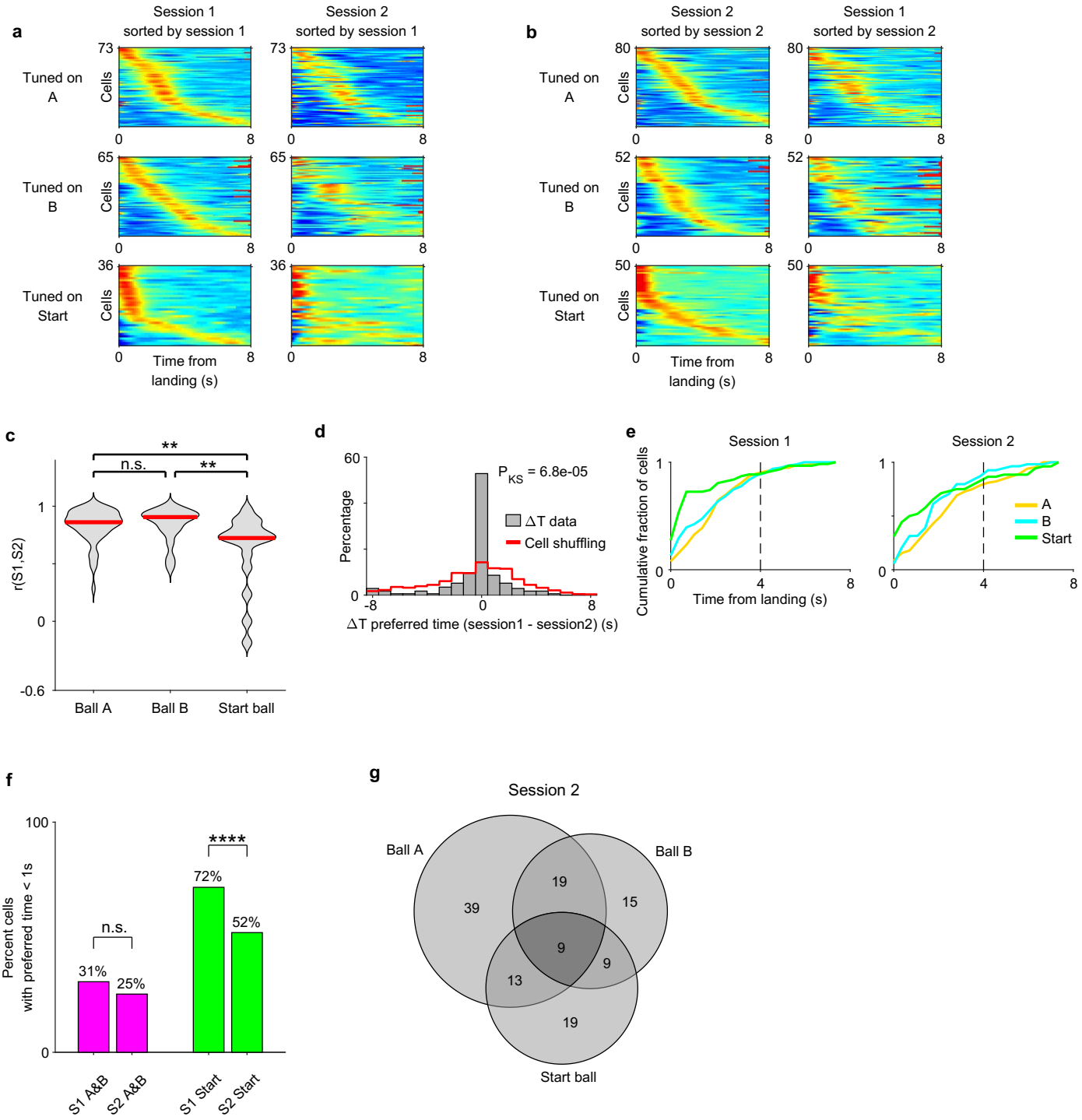

Extended Data Fig. 6 | See next page for caption.

https://doi.org/10.1038/s41593-022-01226-y

Extended Data Fig. 6 | Self time-cells: stability across sessions. In session 1, the observer bat mimicked the flight-choices of the demonstrator bat; in session 2, the observer mimicked an object (Methods). Session 2 was recorded immediately after session 1. This Extended Data Figure shows that the temporal-tuning was generally conserved between the two sessions; however, it also shows that in session 2, the distribution of preferred-times in the Start location became more similar to that in locations A and B (panels a-b: compare the bottom-left panel in b to the two panels above it and to the bottom-left panel in a; and see also panel e – note in session 2 the distributions of preferred-times became more similar across the 3 landing-balls; see below for Kolmogorov-Smirnov tests). The main change in session 2 was a reduction in the percentage of cells with preferred-times < 1-s on the Start ball (panel f: note in session 2 [S2] the green and purple bars were more similar to each other than in session 1 [S1]). This figure suggests that since a major change between session 1 and session 2 was the presence of the demonstrator bat at the Start location in session 1, versus its absence in session 2, this presence/absence may underlie the observed neural differences in the firing sequences between the Start ball and balls A and B in session 1. **(a)** The temporal tuning-curve of time-cells was stable across consecutive sessions. Left column, temporal tuning curves of time-cells that were significantly-tuned in session 1. Cells were sorted according to their preferred time of firing. Right column, temporal tuning curves of the same cells which were tuned in session 1, but plotted for session 2; cells were sorted according to their preferred time in session 1. Note the stability of the internally-generated firing sequences across consecutive sessions (compare left and right panels). **(b)** Same analysis as in panel a, but for significant time-cells in session 2. Panels a and b demonstrate the stability of the sequences over the two sessions. **(c)** Violin plots of the distributions of Pearson correlations between the temporal tuning-curves in the two sessions; we repeated this calculation for each of the three locations. The correlations between the two sessions were very high at locations A and B (medians: ball A, $r = 0.86$, $n = 51$ cells; ball B, $r = 0.91$, $n = 33$ cells), and were statistically indistinguishable between balls A and B (two-sided Wilcoxon rank-sum test, $P = 0.59$; two-sided Kolmogorov-Smirnov test, $P = 0.34$) – indicating stability of the time representation across the two sessions for balls A and B. By contrast, the across-session correlations for the Start location were significantly lower (median on Start: $r = 0.72$, $n = 17$ cells; comparing correlations in A versus Start: two-sided Wilcoxon rank-sum test, $P < 0.002$; two-sided Kolmogorov-Smirnov test, $P < 0.005$; comparing correlations in B versus Start: two-sided Wilcoxon rank-sum test, $P < 0.002$; two-sided Kolmogorov-Smirnov test, $P < 0.002$) – consistent with the explanation that the presence of the demonstrator bat at the Start location in session 1 was responsible for the difference in the firing sequences in session 1 between the Start ball and the other two locations, A and B; note the demonstrator was removed from the room in session 2. **(d)** Gray bars, distribution of differences in preferred-times (ΔT) for the same neuron between session 1 and session 2 (at the same location). Plotted for all the time-cells that were significant in session 1; pooled across the 3 balls ($n = 174$ cells × positions; this number is smaller than the total number of time-cells in this study, because we included here only the significant time-cells where session 2 was run, which was only for a subset of the cells). The sharp peak at $\Delta T = 0$ indicates that the preferred-time of time-cells was stable across sessions. Red line, shuffle distribution (cell shuffling: ΔT for cell i in session 1 minus cell j in session 2, for $i \neq j$; two-sided Kolmogorov-Smirnov test of data versus shuffles, $P = 6.8 \times 10^{-5}$). **(e)** Cumulative distribution functions (CDF) for the preferred-times of the time-cells in each location, for session 1 (left) and session 2 (right) (ball A: yellow; ball B: cyan; Start ball: green). In session 1 the distribution of preferred-times on the Start ball (green) was quite different from those on balls A or B. By contrast, in session 2, the CDF for the Start ball became statistically indistinguishable from the CDFs for balls A and B (two-sided Kolmogorov-Smirnov test on time segments between $t = 0$ and $t = 4$ s: Session 1: Start ball versus ball A: $P = 0.047$; Start ball versus ball B: $P = 0.047$; ball A versus ball B: $P = 0.74$; Session 2: Start ball versus ball A: $P = 0.15$; Start ball versus ball B: $P = 0.37$; ball A versus ball B: $P = 0.74$). Note that we removed the demonstrator bat from the room in session 2, so only in session 1 the observer bat was landing next to the demonstrator bat on the Start ball. Taken together, this suggests that the presence of the demonstrator bat at the Start location in session 1 was responsible for the difference in the firing sequences seen in session 1 between the Start ball and the other two locations, A and B – while in session 2, when the demonstrator was removed from the room, the time-cell sequences became more similar to each other. **(f)** Percentage of time-cells with short preferred-times (< 1 s). Magenta bars, the percentage of time-cells with short preferred-times on balls A and B was statistically indistinguishable between session 1 (S1; $n = 213$ cells) and session 2 (S2; $n = 132$ cells) (two-sided log odds ratio test: $P = 0.055$). Green bars, same for the Start ball: here, the percentage of time-cells with short preferred-times was significantly smaller in session 2 (S2; $n = 50$ cells) than in session 1 (S1; $n = 61$ cells) (two-sided log odds ratio test: $P < 10^{-5}$). Together, panels a-c and e-f suggest that the internally-generated firing sequence on the Start ball became more similar to those on balls A and B during session 2, when the other bat (demonstrator) was absent from the Start-ball and from the room altogether. **(g)** Venn diagram depicting the distribution of time-cell tuning in the different locations, in session 2. Note that we included in this figure only neurons that were stably spike-sorted across *both* sessions (see Methods section on 'Spike sorting').

https://doi.org/10.1038/s41593-022-01226-y

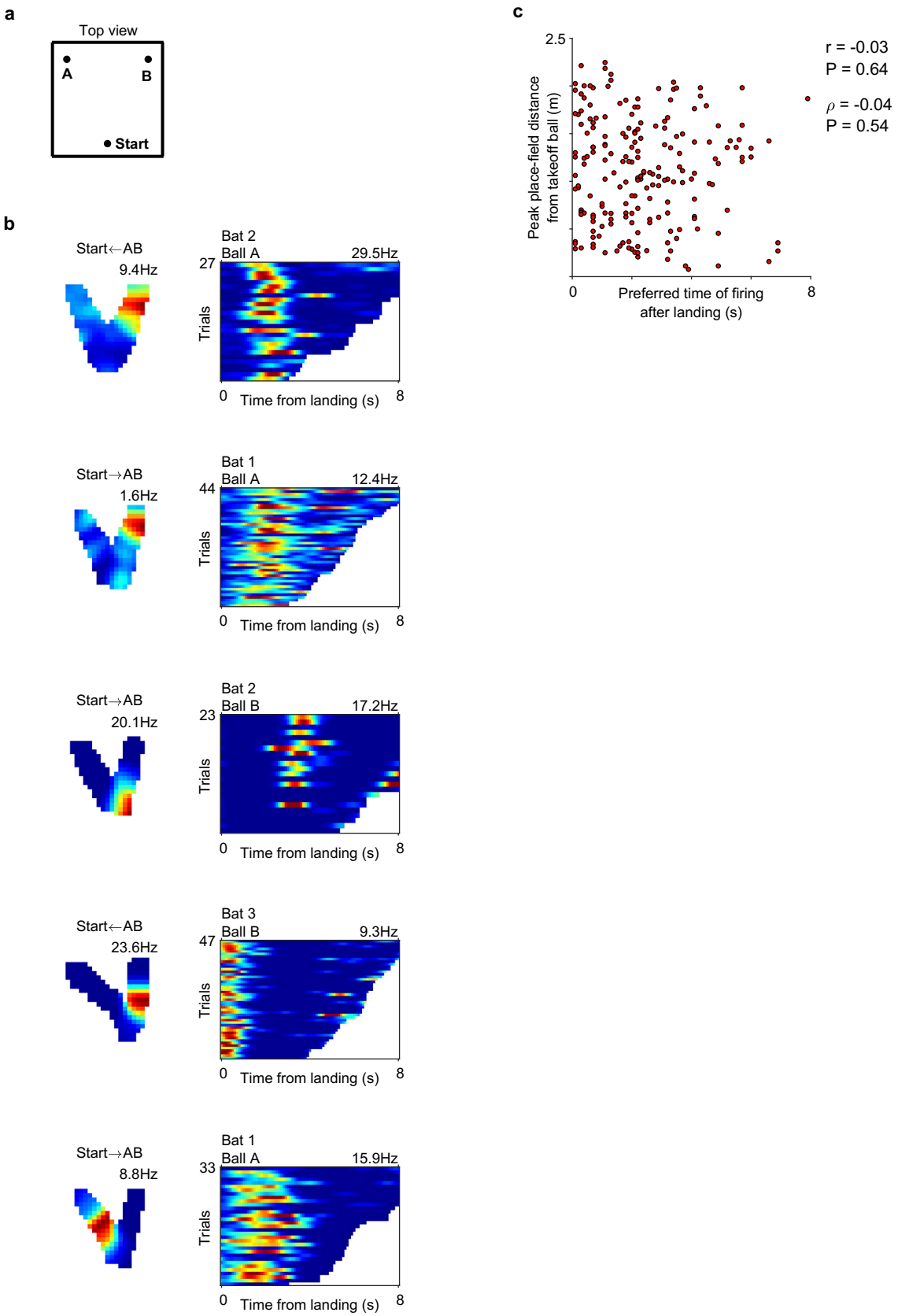

Extended Data Fig. 7 | See next page for caption.

https://doi.org/10.1038/s41593-022-01226-y

Extended Data Fig. 7 | Time-cells (as measured during motionless hanging) and place-cells (as measured in-flight) represent a largely overlapping population of cells – but there was no clear relation between their preferred-time and preferred-place. (a) Top view of the experimental room (2.35 × 2.69 m, with 2.56 m height). Three landing-balls were positioned inside the room, designated as locations 'Start', 'A' and 'B'. **(b)** Five examples of dorsal hippocampal CA1 neurons which were place-cells when the observer bat was flying (left), and were time-cells when the observer bat was motionlessly hanging from one of the landing balls (right). These examples demonstrate two things: First, that time cells and place cells are overlapping populations of cells (see also main Fig. 1h for a population analysis). Second, these examples demonstrate that the place-field and time-field of the same neuron are not necessarily related to each other in a simple way: The top 2 examples are cells whose place-fields were on opposite sides from the location of the time-field; and the bottom 3 examples demonstrate the lack of clear relation between preferred-time and preferred-place – for example late time-field for a cell whose place-field was early along the flight (third from the top), or vice versa (fourth from the top). First example: Left, place-cell firing rate map (top view) for flights from landing balls A and B to the Start ball. Right, time-cell raster for landing ball A. Note that the place-field is located on the flight path from ball B to the Start ball, whereas the time-field is on the other side – on ball A. Second example: Left, place-cell firing rate map for flights from the Start ball to balls A and B. Right, time-cell raster for ball A. Note that the place-field is located on the side of B, while the time-field is on the other side – on ball A. Third example: Left, place-cell firing rate map for flights from the Start ball to balls A and B. Right, time-cell raster for ball B. Note that the place-field is located close to the Start ball – *early* in the flight to B, while the time-field when the bat was on B occurs *late* in time. Fourth example: Left, Place-cell firing rate map for flights from landing balls A and B to the Start ball. Right, time-cell raster for ball B. Note that the place-field is located *mid-way* during the flight from B to Start, while the time-field occurs *early* in time. Fifth example: Left, place-cell firing rate map for flights from the Start ball to balls A and B. Right, time-cell raster on ball A. Note that the place-field is located *mid-way* during the flight, while the time-field occurs relatively *early* in time. **(c)** Population analysis. No significant correlation was found between the preferred time of firing after landing (x-axis) and the distance of the place-field peak from the takeoff-ball (y-axis) (Pearson $r = -0.03$, $P = 0.64$; Spearman $\rho = -0.04$, $P = 0.54$; two-sided tests). Plotted here are all the cells which were both significant place-cells when the bat was flying and significant time-cells when the bat was hanging motionlessly on one of the landing balls ($n = 135$ cells; note the number of dots plotted here [$n = 194$] is larger than the number of cells [$n = 135$] because neurons that had significant place-fields in the two flight-directions have contributed two dots to this scatter, and likewise for cells with significant time-fields in multiple locations [multiple balls]). Overall, there was no strong systematic relation between the preferred-time and preferred-place of firing for bat dorsal CA1 neurons.

https://doi.org/10.1038/s41593-022-01226-y

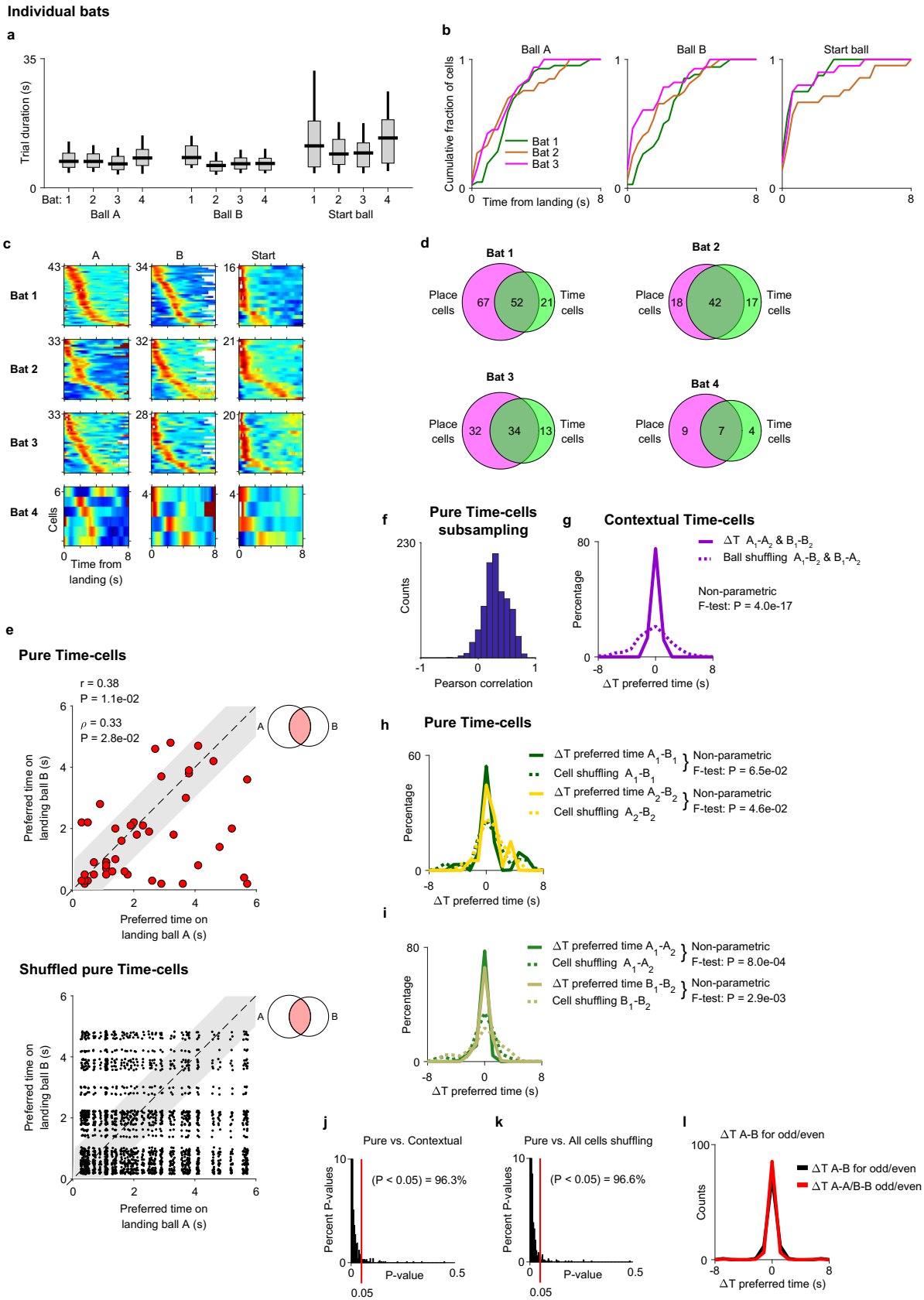

Extended Data Fig. 8 | See next page for caption.

https://doi.org/10.1038/s41593-022-01226-y

Extended Data Fig. 8 | Time tuning across different individual bats, and analysis of pure time-cells. (a-d) Data for individual bats. **(a)** Trial durations at each of the locations in the room (balls A, B and Start), for each of the 4 observer bats which we recorded. Horizontal lines in the box-plots show the median trial duration, boxes show the 25th to 75th percentiles, and vertical lines show the 10th to 90th percentiles. n = 340, 628, 861 and 174 trials on landing ball A, for each of the bats respectively; n = 123, 624, 839 and 119 trials on landing ball B, for each of the bats respectively; n = 439, 861, 1277 and 316 trials on the Start ball, for each of the bats respectively. Mean trial durations for landing ball A: 7.9, 7.7, 7.2, 8.8 s; mean trial durations for landing ball B: 9.1, 6.3, 6.9, 7.1 s; mean trial durations for landing ball Start: 14.5, 10.5, 10.4, 14.7 s. 10th percentile trial duration for landing ball A: 4.0, 4.3, 3.6, 3.8 s; 10th percentile trial duration for landing ball B: 5.4, 3.5, 4.0, 3.9 s; 10th percentile trial duration for the Start ball: 3.9, 3.9, 3.9 4.5 s; 90th percentile trial duration for landing ball A: 12.5, 11.6, 10.9, 14.2 s; 90th percentile trial duration for landing ball B: 14, 9.7, 10.3, 10.6 s; 90th percentile trial duration for the Start ball: 31.7, 17.8, 17.5, 26.1 s. Minimum trial duration for landing ball A: 0.4, 0.3, 0.6, 0.6 s; minimum trial duration for landing ball B: 0.8, 0.3, 0.4, 2.4 s; minimum trial duration for the Start ball: 0.4, 0.6, 0.4, 0.5 s. Maximum trial duration for landing ball A: 23.4, 22.7, 54.2. 59.6 s; Maximum trial duration for landing ball B: 23.3, 19.4, 43.4, 31.3 s; Maximum trial duration for the Start ball: 59.3, 57.1, 56.9, 59.8 s. **(b)** Cumulative functions showing the cumulative fraction of cells with a particular preferred-time for each of the bats no. 1, 2, 3 (the number of cells from bat 4 was low and hence we omitted it from this panel). **(c)** Ensemble temporal sequences for the 3 balls (columns), depicted similarly to main Fig. 1g, but plotted here separately for the 4 bats (rows). **(d)** Venn diagrams showing the distributions and overlap between place-cells and time-cells, separately for each of the 4 observer bats. **(e-f)** Analysis of pure time cells. **(e)** Top panel: Scatter plot showing a significant correlation between the preferred-time on landing ball A and the preferred-time on landing ball B, for all the time-cells which were significantly tuned on both A *and* B in session 1 (Pure time-cells; Spearman rank correlation ρ = 0.33, $P = 2.8\times10^{-2}$; Pearson correlation r = 0.38, P = 0.011; two-sided tests; n = 44 cells; the correlation remained significant also after removing cells with short preferred-time of less than 0.5-s on both balls A and B: Pearson r = 0.32, P = 0.041). Top right inset, Venn diagram illustrating the cell population analyzed here (pink area, time-cells tuned on A *and* B: 'pure time-cells'; n = 44). Bottom panel: Scatter plot for the cell-shuffling of time cells tuned on A *and* B ('pure time-cells'; n = 44) – plotting all possible combinations of the preferred-time of cell i on landing-ball A and the preferred-time for cell j on landing-ball B, where $i \neq$ j, for all the time-cells which were significantly tuned on both A *and* B in session 1 (dots were slightly jittered for display purposes). The Venn diagram illustrates the cell population for the shuffle: as in the top panel. Note that for the majority of the time-cells shown in the top panel (data), the difference between the preferred-times in locations A and B was <1 s (61.4% of the cells [27/44] were within ±1 s from the diagonal – marked by the gray shaded area). This percentage is 2–3-fold larger than expected by chance – when compared to 2 types of chance levels: (i) Only 35.2% [333/946] of the shuffles in the bottom panel were inside the gray band, showing preferred-time differences of <1 s between locations. (ii) Only 22% of the cells are expected to show differences <1 s, assuming uniform distribution of differences (the gray shaded area divided by the total area of the graph = 22%). **(f)** Pearson correlations in panel e (top), after uniform subsampling. Shown is the distribution of Pearson correlations for 1,000 subsamples, which was computed as follows: In panel e (top), we binned the preferred times on ball A (x-axis) into 12 uniform time bins, 0.5 seconds each. Then for each subsample we chose randomly one dot from each bin, to form 12 pairs of preferred times on A and B, whose times on A were uniformly-distributed (by construction). We then calculated the Pearson correlation for these 12 dots. This subsampling procedure was repeated 1,000 times; the distribution of Pearson correlations for these 1,000 subsamples is shown here. The mean Pearson correlation of this histogram was $< r > = 0.31$. We found that 129 correlations out of the total 1,000 correlations showed P-value < 0.05, which amounts to 12.9% of the total subsamples. This fraction of P-values is significantly higher than the fraction of 5% that is expected by chance (one-sided Binomial test: $P < 10^{-300}$). These results further support the notion that pure time-cells preserved their preferred-time between balls A and B. **(g)** Analysis of contextual time-cells. Solid purple: distribution (kernel density plot) of the differences in preferred time for contextual time-cells in both experimental sessions 1 and 2, with differences computed within-ball – for both landing-balls A and B; that is, pooling ΔT preferred times for $A_1 - A_2$ and $B_1 - B_2$ (n = 39 cells × positions). Dashed purple: distribution (kernel density plot) of the shuffled ΔT preferred times between different landing-balls from different sessions: $A_1 - B_2$ and $B_1 - A_2$. These distributions were very significantly different (two-sided nonparametric F-test [Ansari-Bradley test]: $P = 4.0\times10^{-17}$), indicating that contextual time-cells showed stability across sessions, and were more similar between different sessions of the same kind (landing on the same ball) than between different sessions of different kind (landing on different balls). **(h-i)** Comparing pure time-cells across the two sessions. **(h)** Distributions (kernel density plots) of the differences in preferred time for the group of 14 cells which were pure time-cells in both session 1 and session 2. Green, distribution of ΔT between preferred times on ball A versus ball B, for session 1 ($A_1 - B_1$; n = 14 cells; two-sided nonparametric F-test [Ansari-Bradley test] compared to cell-shuffling [dotted line]: $P = 6.5\times10^{-2}$). Yellow, distribution of ΔT between preferred times on ball A versus ball B, for session 2 ($A_2 - B_2$; n = 14 cells; two-sided nonparametric F-test compared to cell-shuffling: $P = 4.6\times10^{-2}$). The cell shuffling distributions (dotted lines) were calculated as the difference between the preferred times for cells i and j, where $i \neq j$. **(i)** Distributions (kernel density plots) of the differences in preferred time for the group of 14 cells which were significant pure time-cells in both session 1 and session 2. Dark green, distribution of ΔT between preferred times in session 1 versus session 2, for ball A ($A_1 - A_2$; n = 14; two-sided nonparametric F-test [Ansari-Bradley test] compared to cell-shuffling [dotted line]: $P = 8.0\times10^{-4}$). Light green, distribution of ΔT between preferred times in session 1 versus session 2, for ball B ($B_1 - B_2$; n = 14; two-sided nonparametric F-test: $P = 2.9\times10^{-3}$). Note that ΔT is strongly and significantly concentrated around ΔT = 0 – suggesting high stability of the pure-time-cell tuning across the two sessions. **(j-k)** Matching the sample size between sets of neural data or between neural data and shuffles. **(j)** Distribution of P-values over 1,000 independent two-sided nonparametric F-tests [Ansari-Bradley tests], where each test was done between the distribution of real ΔT differences (ball A – B, in session 1) of the preferred-times for pure-time cells (n = 44) and randomly chosen 44 samples (neurons), taken from the distribution of ΔT of contextual time-cells. In each of the 1,000 tests the sample size of the pure time-cells and the contextual time-cells was thus identical (matched): n = 44. This distribution shows the percentage (y-axis) of the P-values for each of the 1,000 tests (x-axis); red line indicates the P = 0.05 cutoff. The y-axis was clipped at 10% for display purposes only. Note that 96.3% of the tests yielded P-values smaller then 0.05, indicating that the variance of the distribution of ΔT in pure time-cells was significantly smaller than the variance of the distribution in contextual time-cells – consistent with main Fig. 4c. **(k)** Similar to panel j, but here showing the distribution of P-values between the pure time-cells (n = 44) and 1,000 randomly chosen 44 samples taken from the cells-shuffling distribution of all cells. Note that 96.6% of the tests yielded P-values smaller than 0.05, indicating that the variance of the distribution of ΔT in pure time-cells was significantly smaller than the variance of the distribution for the cells-shuffling – again consistent with main Fig. 4c. **(l)** Distribution of ΔT for pure time cells on balls A and B, compared to a null distribution of shuffles for ΔT using the preferred times on ball A for even trials minus preferred times on ball A for odd trials (and likewise for ball B); plotted for all the pure time cells which exhibited a difference in preferred time of <1 sec (n = 27 cells). The shuffle (null) distribution was significantly different from the data (two-sided nonparametric F-test [Ansari-Bradley test]: $P = 1.4\times10^{-4}$); but nevertheless, the distributions of data (black) and shuffles (red) were clearly highly similar.

https://doi.org/10.1038/s41593-022-01226-y

Time-cells for the other

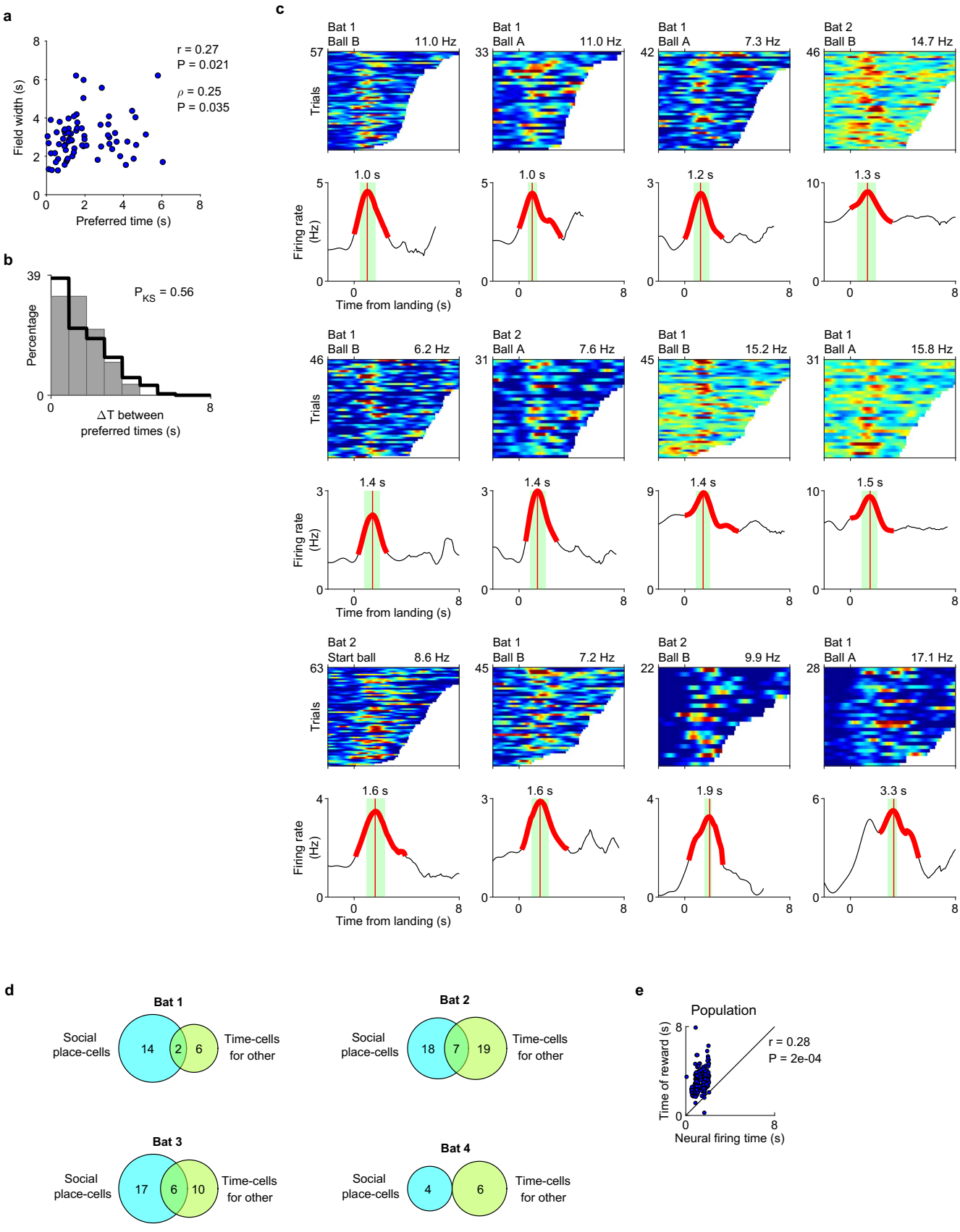

Extended Data Fig. 9 | See next page for caption.

https://doi.org/10.1038/s41593-022-01226-y

Extended Data Fig. 9 | Time cells for the other bat. (a) Scatter plot of the time-field duration (field width at half-height) versus the preferred time, for all the significant time-fields for the other bat, pooled across all three locations (n = 73 significant fields: blue dots; the number of dots here [73] is larger than the number of significant time-cells for the other bat [n = 56], because if a cell was significantly time-tuned on 2 or 3 landing-balls, it contributed 2 or 3 dots to this scatter). This scatter shows a significant positive correlation: Pearson r = 0.27, P = 0.021; Spearman ρ = 0.25, P = 0.035 (two-sided tests). Thus, the resolution of time-fields deteriorated with the passage of time – as for self time-cells (Extended Data Fig. 2d), and as reported for time-cells in rats[7,8,10,17]. **(b)** Firing sequences in simultaneously-recorded time-cells for the other bat are similar to the population time-cell sequences pooled across all days. Distributions of time-differences (ΔT) between the preferred-times for all the pairs of significant time-cells for the other, which were recorded simultaneously on the same day (gray bars; n = 28 cell-pairs), and all the cell-pairs recorded on different days (black line; n = 1672 cell-pairs), pooled over the 3 locations in the room. The gray and black distributions were statistically indistinguishable (two-sided Kolmogorov-Smirnov test: P = 0.56). This demonstrates that the pooled sequences for time-cells for the other bat (main Fig. 5c: diagonal panels) are reliably representing the within-day sequences – indicating that time-cells for the other bat form internally-generated firing sequences. **(c)** Additional 12 examples of time-cells for the other. For each example cell, the top panel shows the color-coded raster plot: x-axis, elapsed time from the moment the bat has landed (time 0); y-axis, repeated landings (trials); plotted as in main Fig. 1e. The bottom panel shows the temporal tuning-curve (black trace), which is the averaged firing-rate of each cell (average of the color-coded raster above); the preferred-time is indicated above the peak-firing of each cell (marked also by a vertical red line); green shading represents statistically-significant time bins; red curve shows the width-at-half-height of the time-field. **(d)** Venn diagrams showing the distributions and overlap between social place-cells and social time-cells, separately for each of the 4 individual recorded bats. (**e**) Scatter plot of the time of peak firing of the time-cells for the other bat versus the time of reward (dots show individual trials, pooled across all the example cells shown in main Fig. 5; Pearson r = 0.28; $P = 2 \times 10^{-4}$; two-sided test; n = 174 trials). Note there was large variability in the time-of-reward (large spread along the y-axis: standard deviation = 1.0 s; mean = 3.18 s), which was substantially larger than the variability in the neurons' time of firing across the trials (small spread along the x-axis: standard deviation = 0.45 s; mean = 1.38 s).

nature portfolio

Corresponding author(s): Nachum Ulanovsky, David Omer

Last updated by author(s): Oct 23, 2022

Reporting Summary

Nature Portfolio wishes to improve the reproducibility of the work that we publish. This form provides structure for consistency and transparency in reporting. For further information on Nature Portfolio policies, see our Editorial Policies and the Editorial Policy Checklist.

Statistics

For all statistical analyses, confirm that the following items are present in the figure legend, table legend, main text, or Methods section.

n/a	Confirmed
☐	☒ The exact sample size (*n*) for each experimental group/condition, given as a discrete number and unit of measurement
☐	☒ A statement on whether measurements were taken from distinct samples or whether the same sample was measured repeatedly
☐	☒ The statistical test(s) used AND whether they are one- or two-sided *Only common tests should be described solely by name; describe more complex techniques in the Methods section.*
☒	☐ A description of all covariates tested
☐	☒ A description of any assumptions or corrections, such as tests of normality and adjustment for multiple comparisons
☐	☒ A full description of the statistical parameters including central tendency (e.g. means) or other basic estimates (e.g. regression coefficient) AND variation (e.g. standard deviation) or associated estimates of uncertainty (e.g. confidence intervals)
☐	☒ For null hypothesis testing, the test statistic (e.g. *F*, *t*, *r*) with confidence intervals, effect sizes, degrees of freedom and *P* value noted *Give P values as exact values whenever suitable.*
☒	☐ For Bayesian analysis, information on the choice of priors and Markov chain Monte Carlo settings
☒	☐ For hierarchical and complex designs, identification of the appropriate level for tests and full reporting of outcomes
☐	☒ Estimates of effect sizes (e.g. Cohen's *d*, Pearson's *r*), indicating how they were calculated

Our web collection on statistics for biologists contains articles on many of the points above.

Software and code

Policy information about availability of computer code

Data collection	Neural data acquisition was done using a wireless neural logger (SpikeLog-16, Deuteron Technologies), accelerometer data acquisition was also done using the neural logger, video tracking was done using Neuralynx Cheetah VTS, advancing tetrodes and screening for neurons was done using Neuralynx DigitalLynxSX and Neuralynx Cheetah (version 6.3.0).
Data analysis	Spike sorting was done using SpikeSort3D (version 2.5.2.0; Neuralynx). We used MATLAB (version 2021b) custom code for data analysis. The code will be made available upon a reasonable request from the authors, and is also accessible online at Zenodo (see link in ref. 46).

For manuscripts utilizing custom algorithms or software that are central to the research but not yet described in published literature, software must be made available to editors and reviewers. We strongly encourage code deposition in a community repository (e.g. GitHub). See the Nature Portfolio guidelines for submitting code & software for further information.

Data

Policy information about availability of data

All manuscripts must include a data availability statement. This statement should provide the following information, where applicable:

- Accession codes, unique identifiers, or web links for publicly available datasets
- A description of any restrictions on data availability
- For clinical datasets or third party data, please ensure that the statement adheres to our policy

Data will be made available from the authors upon a reasonable request, and are also accessible online at Zenodo (see link in ref. 46).

Human research participants

Policy information about studies involving human research participants and Sex and Gender in Research.

Reporting on sex and gender	N/A
Population characteristics	N/A
Recruitment	N/A
Ethics oversight	N/A

Note that full information on the approval of the study protocol must also be provided in the manuscript.

Field-specific reporting

Please select the one below that is the best fit for your research. If you are not sure, read the appropriate sections before making your selection.

☒ Life sciences ☐ Behavioural & social sciences ☐ Ecological, evolutionary & environmental sciences

For a reference copy of the document with all sections, see nature.com/documents/nr-reporting-summary-flat.pdf

Life sciences study design

All studies must disclose on these points even when the disclosure is negative.

Sample size	No power analysis was used to pre-determine the sample size: neither for the number of animals nor for the number of neurons. The numbers of animals and neurons are typical for studies in this research field, in both rodents and bats (e.g. refs. 6, 7, 42-44 in the paper).
Data exclusions	No animals and no data points were excluded from the analyses in this study – except as described in the Methods section "Definition of time cells", where we defined the inclusion criteria for time cells. The inclusion criteria for time cells were based on sufficient number of trials, sufficient time on the landing-balls, sufficient number of spikes, significant response, and firing stability.
Replication	The effects described were confirmed in multiple cells recorded over multiple recordings sessions in 4 animals.
Randomization	Not relevant, as there was no randomized treatment of the animals: This study is based on observing the neural responses during free behavior of the animals.
Blinding	The investigators were not blinded to the animal identity. Analysis of neural and behavior data was conducted regardless of the identity of the animal from which the data were collected.

Reporting for specific materials, systems and methods

We require information from authors about some types of materials, experimental systems and methods used in many studies. Here, indicate whether each material, system or method listed is relevant to your study. If you are not sure if a list item applies to your research, read the appropriate section before selecting a response.

Materials & experimental systems

n/a	Involved in the study
☒	☐ Antibodies
☒	☐ Eukaryotic cell lines
☒	☐ Palaeontology and archaeology
☐	☒ Animals and other organisms
☒	☐ Clinical data
☒	☐ Dual use research of concern

Methods

n/a	Involved in the study
☒	☐ ChIP-seq
☒	☐ Flow cytometry
☒	☐ MRI-based neuroimaging

Animals and other research organisms

Policy information about studies involving animals; ARRIVE guidelines recommended for reporting animal research, and Sex and Gender in Research

Laboratory animals	Egyptian fruit bats (Rousettus aegyptiacus). Sex: male. Age: adult, 2 - 10 years old.
Wild animals	The bats in this study (8 male Egyptian fruit bats, Rousettus aegyptiacus) were captured as adults in Israel, using butterfly nets. They were transported in a car to the Weizmann Institute, where they were quarantined and then joined a large bat colony at the Institute. Following experiments, the 4 bats from which we conducted neural recordings were euthanized with pental for purpose of brain histology.
Reporting on sex	This study used only male bats.
Field-collected samples	The study did not involve samples collected from the field
Ethics oversight	The experimental procedures described in this study were approved by the Institutional Animal Care and Use Committee (IACUC) of the Weizmann Institute of Science - as also stated in the Methods (section "Surgery and recording techniques").

Note that full information on the approval of the study protocol must also be provided in the manuscript.